J. Fluid Mech. (1992), *vol.* 241, *pp.* 469–502
Printed in Great Britain

The structure of a turbulent free shear layer in a rotating fluid

By A. A. BIDOKHTI† AND D. J. TRITTON‡
Department of Physics, University of Newcastle upon Tyne, NE1 7RU, UK

(Received 3 January 1990 and in revised form 22 January 1992)

An experimental investigation has been carried out on the effects of rotation on the development and structure of turbulence in a free shear layer, oriented so that its mean vorticity is parallel or antiparallel to the system vorticity. The effective local Rossby number extended down to about $\frac{1}{3}$. The experimental methods were hydrogen-bubble flow visualization and hot-film anemometry.

In summarizing the results we refer to stabilized flow when the system vorticity has the same sign as the shear vorticity and destabilized and subsequently restabilized when it has the opposite sign (Tritton 1992). The roller eddy pattern, familiar in non-rotating flow, was observed in all stabilized flows, but was almost completely disrupted by even weak destabilization. Notable features of the quantitative results were: reorientation by Coriolis effects of the Reynolds stress tensor (inferred from the ratio of the cross-stream to longitudinal turbulence intensity and the normalized shear stress); changes in the ratio of spanwise to longitudinal intensity similar to but weaker than changes in the ratio of cross-stream to longitudinal; a gradual decrease, with increasing stabilization, of the Reynolds shear stress leading ultimately to its changing sign; an increase of the Reynolds shear stress in the destabilized range followed by rapid collapse to almost zero with restabilization. Absolute intensities did not change in line with the turbulence energy production, implying enhancement of dissipation in destabilized flow and inhibition in stabilized and restabilized. Correlation measurements indicated changes of lengthscale in the spanwise direction, and spectra indicated changes in the longitudinal direction that suggest that this enhancement and inhibition are associated with variations between fully three-dimensional and partially two-dimensional turbulence. Data for a wake in a rotating fluid (Witt & Joubert 1985) show similarities to some of the above observations and can be incorporated into the interpretation.

1. Introduction

This paper reports laboratory experiments on the effect of rotation of the whole system on the structure of a turbulent flow. Reviews of the contribution of previous such experiments to our knowledge and understanding of the ways in which Coriolis effects change turbulent flows have been given by one of the present authors (Tritton 1978, 1985) and by Hopfinger (1989). Most of this work has been motivated by the need for this knowledge and understanding in many aspects of geophysics, planetary physics and astrophysics, although there are also engineering applications. For the

† Present address: Atomic Energy Organisation of Iran, P.O. Box 14155-1339, Tehran, Iran.
‡ Present address: Institut de Mécanique de Grenoble, Domaine Universitaire, B.P.53X, 38041 Grenoble Cedex, France.

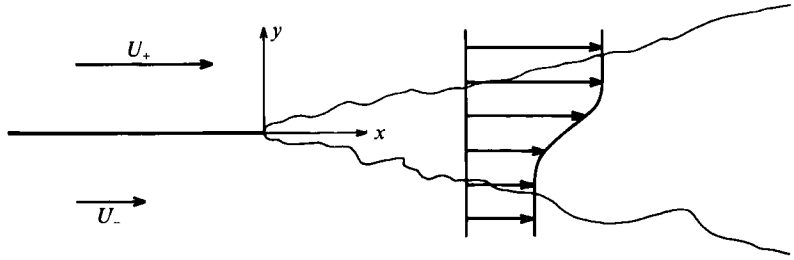

FIGURE 1. The flow configuration.

most part, the motivation has not been a particular topic within these applied sciences so much as a whole range of topics to which the ideas are generally applicable. The present work continues in this tradition.

The configuration investigated is shown schematically in figure 1 (which includes the coordinate system used throughout this paper). Two parallel streams at different speeds, U_+ and U_-, meet at the end of a splitter plate. A shear layer forms between the two streams, spreading with distance downstream. Instability of the shear layer leads to it being turbulent. The whole system may be rotated, in either sense about an axis perpendicular to the plane of figure 1. Ideally, the mean flow is two-dimensional, with neither the mean flow nor the turbulence being influenced by endwalls in the perpendicular (z) direction. The shear vorticity is thus parallel or antiparallel to the system vorticity. This means that it is in principle possible for the mean flow not to be directly changed by Coriolis effects. These do, however, act on fluctuations superimposed on the mean flow, thus affecting the process of transition to, and the structure of, turbulent motion (which may, of course, indirectly affect the mean flow), as discussed in an accompanying paper (Tritton 1992).

The pioneering work on the effect of rotation on shear flow turbulence (with mean flow vorticity parallel or antiparallel to rotation vorticity) was that by Johnston, Halleen & Lezius (1972) on channel flow. As discussed in Tritton (1992), they developed many of the main ideas for interpretation of such experiments as well as obtaining a valuable body of experimental data. Subsequent closely related experiments were those on boundary layers by Koyama *et al.* (1979) and Watmuff, Witt & Joubert (1985). Rothe & Johnston (1975, 1979) investigated the effects of rotation on a free shear layer between a separation point and reattachment. They were primarily concerned with the overall flow pattern, in particular the effect of rotation on the position of reattachment. They did, however, make some flow visualizations which are very informative and to which we shall refer in §7.2. Witt & Joubert (1985) investigated a wake in a rotating fluid. There are ways in which it is particularly appropriate to compare their results with ours; see §6.2.

Numerical experiments have been performed relating to homogeneous shear flow (Bertoglio 1982; Speziale & Mac Giolla Mhuiris 1989) and channel flow (Andersson *et al.* 1988; Kristoffersen & Andersson 1992). More recent numerical experiments (direct simulations by Lesieur, Yanase & Métais 1991 and modelling by Nilsen & Andersson 1991) concern shear layers. Both these papers refer to the present work (on the basis of Bidokhti & Tritton 1990) and Nilsen & Andersson include some quantitative comparisons. Both numerical projects are continuing (private communications) and fuller comparison will be important in due course. For the moment we just occasionally note below points of similarity and difference.

In all the above laboratory experiments, the effect of rotation has been either

weak or moderate. This is indicated by considering maximum typical values of $|S|$ (maximum with respect to different cases – rotation rate, distance downstream, etc.; typical for that case). S is defined in Tritton (1992) and again in §3 below, but it may be thought of as the reciprocal of the appropriate form of Rossby number. With the exception of the wake experiments, this maximum was always less than about 0.25; in the wake it was about 1.1 (see figure 16 below). One objective of our own experiments has been to achieve stronger rotational effects. $|S|$ extends up to about 3 (figure 16), though the results became less reliable at its larger values. Rotational effects thus become strong although never dominant.

The other experiments providing relevant background information are those on turbulent free shear layers without rotation. Measurements of turbulence quantities with which one might compare our data are those surveyed by Rodi (1975) and those of Saiy & Peerless (1978), Oster & Wygnanski (1982), Badri Narayanan & Raghu (1982) and Mehta *et al.* (1987) (the values of U_-/U_+ being comparable with ours). The discrepancies within these data are substantial and suggest strong sensitivity to small, usually uncontrolled changes in flow conditions, as is confirmed by specific observations of changes brought about by changing the upstream conditions (Browand & Latigo 1979) or the free-stream turbulence level (Pui & Gartshore 1979).

It is known from flow visualization experiments that a prominent feature of shear layers over a very wide Reynolds-number range is the occurrence of cross-stream vortices or 'roller eddies', like those generated by Kelvin–Helmholtz instability (Brown & Roshko 1974; Roshko 1976; Cantwell 1981). More recent observations have revealed various smaller-scale effects superimposed on these (Breidenthal 1981; Jimenez 1983; Bernal & Roshko 1986; Lasheras, Cho & Maxworthy 1986). Some of these features are Reynolds-number dependent and one might say that they concern transitional rather than fully turbulent flow. There has been controversy (e.g. Chandrsuda *et al.* 1978) as to how this distinction should be made for free shear layers, and the recent work has complicated rather than clarified this question. The flow becomes turbulent (in the sense, say, that the velocity fluctuates in a way characteristic of turbulent flow) long before it becomes fully developed (in the sense of Reynolds-number independence).

The Reynolds numbers Re of our experiments fall within this range (roughly 10^3 to 10^5 for Re as defined in §3) where the flow is 'turbulent but developing'. This, combined with the sensitivity to small changes, means that there is no well-defined non-rotating flow as a point of reference. Our approach has been to make direct comparison between the flows in our apparatus at various rotation rates, including zero (although this does not completely circumvent the problem, because the rotation may alter quantities or features to which the flow is sensitive; see e.g. §7.4).

We selected the free shear layer for our experiments, despite the above disadvantage, because it is in a sense the simplest of shear flow configurations and, more specifically, because it seems a good context in which to explore the consequences of the stabilizing and destabilizing processes discussed in Tritton (1992). In particular, the fact that the mean flow vorticity has the same sign throughout, and thus that the parameter S does also, makes application of the ideas in that paper more straightforward.

A more detailed account of this work is available in a separate report (Bidokhti & Tritton 1990).

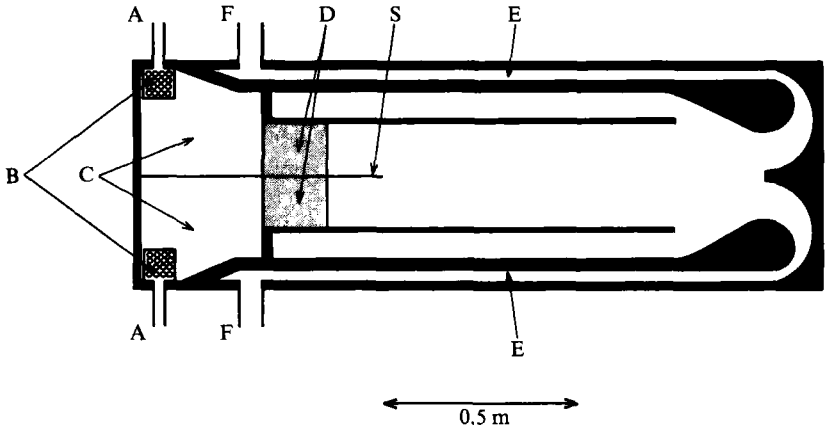

FIGURE 2. Horizontal section of the flow channel.

2. Apparatus and procedures

The working fluid is water. The essential features of the flow channel and its dimensions are shown schematically in plan view (perpendicular to the rotation axis) in figure 2, which is to scale. The working section has a uniform depth of 0.32 m and a width of 0.27 m. The walls of the channel are of Perspex.

The shear layer is formed between two parallel streams meeting at the end of splitter plate S. The two flows are completely separated upstream of this, each entering through a pipe A via a perforated box B into a settling chamber C and then passing through a smoothing section D, consisting of 25 mm of foam, 150 mm of honeycomb and a gauze. The splitter plate is 7 mm thick but tapers in the last 40 mm to a point. At the downstream end of the working section the flow is again divided; water passes through side-channels E and is returned from outlets F through pumps to the inlets. All parts of the flow system except the inlet and outlet pipes have the same depth as the working section.

The flow rates are controlled in two ways. First, a by-pass valve connected directly across each pump allows a variable amount of pumped water to be diverted from the channel. Secondly, one of the pumps, normally that used for the slower flow rate, can be driven at a variable speed.

The whole channel including the pumps and by-pass valves, but not the speed controller or other electronic circuitry, is mounted on a table, which can be rotated in either sense at rates in the range 1.6 to 16 r.p.m., with a stability of about 1 part in 1000.

Flow visualization used the hydrogen-bubble technique. A platinum wire of 80 μm diameter was stretched across the channel in the transverse (y) direction, 5 mm downstream of the end of the splitter plate. This wire was maintained throughout the experiments and all the photographs in figures 3–7 show bubbles released from it. Bubble wires further downstream and at different depths were used in preliminary experiments to examine the general structure of the flow, but these were either allowed to lapse when they broke or removed when they obstructed probes. Also used in the preliminary explorations was a vertical wire mounted on a movable frame.

A voltage of 50 V was applied between the wire(s) and two large copper electrodes on the channel sidewalls. The wire voltage could either be maintained to generate bubbles continuously or be pulsed to produce strips of bubbles. Although the wire was nominally uniform there was a tendency for bubbles to be formed preferentially

at some sites; the consequent variations in bubble sheet intensity actually improved the clarity of the pictures. It was found that the effectiveness of bubble production was improved by occasionally reversing the polarity and so generating oxygen bubbles at the wire.

A television camera and a still camera with an automatic winder were mounted above the tank on a frame rotating with it. The picture from the former was displayed on a monitor screen.

Quantitative measurements of the flow were made with hot-film anemometers (Dantec types 55R32 and 55R72). Straight wedge films were used for sensing the longitudinal velocity (mean and fluctuation) and V-array wedge films, in different orientations, for all three fluctuation components. Two channels of anemometry were available; thus, two straight probes could be used for correlation measurements of the longitudinal velocity fluctuations, but only one V-probe could be used at a time.

Probes were introduced through slots in the top of the channel. By having three slots and mounting stems of different lengths, a probe could be set at various distances downstream. A probe was set up at fixed values of x and z, and traversed by a stepping motor through the shear layer in the y-direction. Its position was known by viewing it against a scale through the closed-circuit TV.

Only one probe could be traversed in this way. Consequently, during the use of two probes for correlation measurements, one of them had to be positioned entirely manually. This was a very slow procedure, and so only a very limited number of correlation measurements has been made.

The probes were operated in the constant-temperature mode, normally at about 30 °C above the water temperature. Occasional adjustment was needed to allow for a gradual rise in water temperature, due to dissipation in the pumps, during a run.

Probe calibration used the spacing of bubble lines generated at a known frequency and photographed to a known scale as a measure of the flow speed. This was done with the apparatus non-rotating and with the probe moved into a region outside the shear layer. (Taking a photo and measuring the anemometer output were thus sequential, as having the probe connected whilst bubbles were being generated could damage it.)

Calibration was a somewhat troublesome process involving moving the probe from its measuring location. We therefore carried out quite long sequences of observations without calibration checks. This was acceptable because there were other reasons, to be discussed in §6.1, why relative measurements (such as ratios of turbulence intensity components or the normalized Reynolds stress) were more accurate than absolute ones. Much of our interpretation focuses attention on the former. Uncertainties of calibration are of much less importance in the determination of relative values.

The techniques for processing the anemometer outputs to give flow quantities were entirely conventional. With the exception of the determination of spectra, they were all analogue techniques. The bandwidth for the fluctuation measurements was usually 0.1 Hz to 1.5 kHz. Spectra were determined digitally from samples of the anemometer signal at 2048 equally spaced times.

Connection between equipment on the rotating table and that off it is via slip-rings. Brass rings with carbon brushes are used for providing power to the pumps, camera and traverse motors, and lighting. Silver rings with carbon brushes are used for transmitting the closed-circuit TV and hot-film anemometer signals.

Fuller description of the apparatus and its use, with reasons for some of the features, is given in Bidokhti & Tritton (1990).

3. Specification

For the ideal configuration of figure 1, there are three governing non-dimensional parameters: the velocity ratio U_-/U_+; the Reynolds number

$$Re = (U_+ - U_-)x/\nu$$

(ν being the kinematic viscosity); and a parameter involving the rotation rate Ω

$$Q = -2\Omega\, x/(U_+ - U_-).$$

$(U_+ - U_-)$ is the appropriate velocity scale in Re and Q because all the dynamical processes under investigation depend on there being a velocity gradient between the two sides. The reason for the sign of Q will be explained below.

Using these parameters to specify conditions in an experiment assumes that x, the distance downstream from the end of the splitter plate is the only relevant lengthscale; i.e. that the shear layer has no initial thickness at $x = 0$ and that all other walls are remote. Possible consequences of non-fulfilment of this assumption will be considered below and in §4.

We intended to keep the velocity ratio constant in our experiments. For the quantitative measurements a value of around 0.4 proved most suitable (as a compromise between suppressing wall attachment and reducing uncertainty in $(U_+ - U_-)$). Many of the photographs to be shown have a higher value of U_-/U_+, typically around 0.65. (They were taken before the pump speed controller was introduced; lower values of U_-/U_+ could not be obtained by use of the by-pass valves alone.)

The Reynolds number may be expected to be of minor importance provided it is large enough. However, we have seen in §1 that, for $\Omega = 0$, it does still have some effect for the values of our experiments.

Q is by far the most important of the governing non-dimensional parameters, as a measure of the importance of rotation. The form of Q shows that increasing the rotation rate and going further downstream have corresponding effects. Quantitatively, Q may not scale these alternatives entirely correctly, because of Reynolds-number effects and because of the initial thickness of the shear layer due to the boundary layers on the splitter plate. Qualitatively, however, one would expect them to be equivalent. Thus for a particular flow, the relative effect of rotation increases with distance downstream.

This can be related to the general effects of rotation on shear flows reviewed in Tritton (1992). The important parameter there is the ratio of the system vorticity to the shear vorticity

$$S = -\frac{2\Omega}{\partial U/\partial y}.$$

In the present flow S varies both across the shear layer and with distance downstream. At a given x, we define

$$S_0 = -4\Omega\delta_M/(U_+ - U_-),$$

where δ_M is the distance between the positions at which $(U - U_-)/(U_+ - U_-) = 0.25$ and 0.75 (see §6.4). S_0 is thus a value of S based on the average velocity gradient in the central part of the profile. (The choice of δ_M as a measure of the width of the profile was made partly as the one that could be determined with least uncertainty. The local value of $|S|$ at the centre of the shear layer where $\partial U/\partial y$ is maximum is typically

10% smaller than $|S_0|$. A value based on the average gradient in the region in which 90% of the velocity variation occurs is typically 30% larger than $|S_0|$.)

The increasing relative effect of rotation with distance downstream now corresponds to increasing $|S_0|$ (decreasing local Rossby number), essentially because the shear layer thickens with distance downstream. The scaling considerations above imply that primarily

$$S_0 = S_0(Q)$$

(for fixed U_-/U_+). It is useful to have a rough general indication of the size of S_0, as the most immediate measure of the importance of rotation. For this purpose one may take

$$S_0 = Q/7$$

in our experiment. (More precisely how it varies will be considered around figure 16.)

The sign of Q has been chosen so that it is the same as that of S_0 and thus the sign of S throughout the flow (with the convention that U_+ is on the positive-y side of the shear layer and U_- on the negative-y side). Consequently on the basis of ideas in Tritton (1992), positive Q implies that the effect of rotation will be increasingly stabilizing as one goes downstream; negative Q implies that it will be initially destabilizing and subsequently restabilizing. Corresponding developments are to be expected at fixed x as the rotation rate is increased.

In the experiments the fast side was normally on the positive-y side (as shown in figure 1). The sign of Q was changed by reversing the rotation: clockwise for positive Q, anticlockwise for negative. All the photographs we shall show will be for this arrangement.

4. The flow: general aspects

The question obviously arises as to how well the actual flow corresponds to the ideal one of figure 1.

Boundary layers on the splitter plate influence the initial formation of the shear layer. These boundary layers may be modified by rotation and thus this initial influence changed. The parameter S will have the same sign as in the shear layer itself in the boundary layer on the fast side, the opposite sign in the boundary layer on the slow side. The distance from the end of the smoothing system to the end of the splitter plate was kept small so that these boundary layers would be thin; it might be hoped that they were laminar. Nevertheless, fluctuations were observed in them, probably due to upstream disturbances not being fully removed by the smoothing. Moreover, these fluctuations were changed by rotation in the ways to be expected. A hot-film probe was introduced into each boundary layer 50 mm upstream from the end of the splitter plate and about 3 mm from it. Mean-square velocity fluctuation readings were made with the apparatus not rotating and with it rotating at 0.43 rad s^{-1} in either sense. In the boundary layer on the fast side, clockwise rotation (corresponding to positive S) reduced the intensity to 36% of its non-rotating value; anticlockwise rotation increased it to 155%. On the slow side, clockwise rotation (negative S) increased it to 520% and anticlockwise reduced it to 62%. Without fuller probing of the boundary layers, the actual figures are of little significance. They do, however, show that the boundary layers were modified by the rotation.

The boundary layers on the sidewalls of the channel are similarly affected, and, in particular, the destabilized boundary layer spreads more rapidly. Concern about the effects of this limited the maximum x at which observations were made. The effect

on the mean flow contributes to uncertainty in the effective U_+ or U_- 'seen' by the shear layer (see also below and §6.1) and may introduce dynamically significant dU_+/dx or dU_-/dx. Consideration of the latter effect (Bidokhti & Tritton 1990) indicates that it is entirely negligible in the region of the photographs in §5; but the external velocity gradient may be of the order of 10% of $\partial U/\partial x$ within the shear layer at the largest x where most of the measurements in §6 were made. This will have had some effect on the spreading of the shear layer (figure 15). Assuming that inferences may be based on observations of non-rotating flows, information in Rodi (1975) suggests that the effect on turbulence structure will have been much less.

The boundary layers on the top and bottom of the channel are Ekman layers. These will interact with the shear layer through the Ekman suction/injection process, producing a secondary circulation with vertical motion in the shear layer. The design criterion for this not to be a serious cause of departure from the ideal flow pattern was that the time of passage of water through the channel should be short compared with the spin-up time; the ratio never exceeded about 1/20. The spin-up time was estimated on the assumption that the Ekman layers were laminar. The Reynolds number of each Ekman layer varied between 30 and 250 (with values at the lower end of the range for the most rapid rotation, when the spin-up time is shortest), compared with its critical value of 55. The layers will thus often have been unstable but are unlikely to have been fully turbulent. Hence, the spin-up time may be overestimated, but probably not seriously. The implication is that the secondary circulation should not have modified the mean flow seriously within the range of the experiments, but is a reason (amongst others) for not attempting to achieve higher values of $|Q|$. By symmetry the effect will be minimum at mid-height where all the measurements presented in §6 were made.

In principle, interaction with the Ekman layers could act directly on the turbulence as well as on the mean flow. This will be important at mid-height only if the turbulence spanwise lengthscale ceases to be small compared with the depth. Correlation measurements to be presented in figure 17 provide information on this. The largest value of $r_z/x = 0.29$ corresponds to $r_z = 0.12$ m, i.e. 0.75 times the distance to the top or bottom from the level at which observations were made. Non-zero but small correlation coefficients observed for this separation imply that there may be some influence of the Ekman layers on the observed turbulence but not a dominant one. Extrapolation suggests that this may be a significant effect towards the end(s) of our Q-range but not for most of our observations. (There are no relevant correlation measurements for negative Q but if there is an effect for positive Q there may also be one for negative.)

The overall structure of the flow was examined using the horizontal bubble wires in various positions and the moveable vertical one mentioned in §2, looking for both imperfections due to the above causes and unexpected ones. Such departures as there were from the ideal flow were rather complicated and difficult to describe; they appeared to relate more to uncontrolled imperfections than to an Ekman-layer-driven secondary flow. A decision that a flow is 'acceptable' is a somewhat subjective one. However, these experiments established that there were no gross imperfections preventing the shear layer from being the dominant flow non-uniformity in the region studied.

Pulsing of the principal bubble wire enabled more specific study of the mean velocity distribution around the shear layer. An example is given in figure 3 (which shows about $\frac{2}{3}$ the width of the channel); further examples are given in Bidokhti & Tritton (1990). The quality of the flow tended to deteriorate as the rotation rate

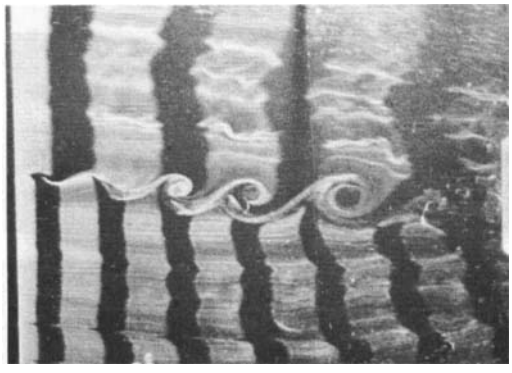

FIGURE 3. Example of the flow field ($\Omega = -0.52$ rad s^{-1}).

increased. There was a general trend for the rotation to induce shear, with vorticity of opposite sign to the rotation, in the regions supposedly outside the shear layer, as can be seen particularly in the bottom half of figure 3. (A qualitative explanation of this in terms of changes in the pressure difference across the smoothing section, due to Coriolis forces, is given in Bidokhti & Tritton 1990.) Additionally, less systematic variations occurred, complicating and sometimes masking the above. Small imperfections in the velocity distribution for $\Omega = 0$, perhaps due to irregularities in the smoothing section, usually became more marked when $\Omega \neq 0$. The velocity gradients involved, both systematic and otherwise, were always small compared with the maximum gradient in the shear layer, but they did sometimes make the edge of the shear layer ill-defined and introduce uncertainty into the effective values of U_+ and U_-.

It was also observed that rotation sometimes resulted in the mean flow not being straight down the channel and/or the shear layer being slightly curved. This will be apparent in some of the photographs in §5. Systematic trends with rotation rate were not apparent, and the reason for this variable behaviour is not known. During the quantitative measurements the centre of the shear layer was located by the velocity measurements but was usually within 10 mm and always within 25 mm of the channel centre (at $x = 0.43$ m), again with no systematic dependence on the rotation.

The flow visualization indicated that the principal departures of the mean flow from the ideal were spatial, not temporal; i.e. the departures outlined above were steady features, with any fluctuations in U_+ or U_- being much smaller. However, there was a tendency for the background turbulence level in the regions outside the shear layer to increase with increasing rotation rate. This was probably a consequence of the less uniform mean velocity distribution.

5. Results: flow visualization

In figures 4–6 each picture is a plan view of a horizontal (x, y)-plane with the bubble release wire at the left-hand side and the end of the splitter plate just out of the picture to the left. In viewing these, one needs to remember that the channel width is much larger than the field of view; cf. figure 3. The faster flow is always to the top of the picture. All pictures are to the same scale. The distance from the bubble wire to the white line near the right edge of most of the pictures is 0.23 m. (This white line is on the lid of the apparatus slightly off-centre. The different appearance of a few of the pictures is because these were taken after the introduction of slots for

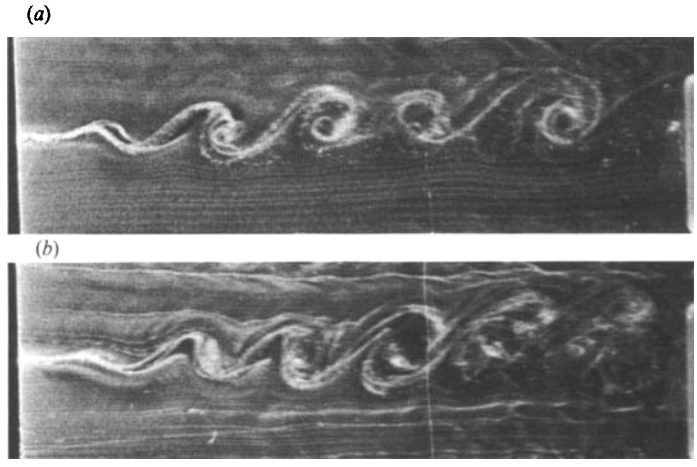

FIGURE 4. Two examples of the shear layer without rotation.

the probes; there was no change within the flow.) Hence, the Reynolds number $(U_+ - U_-)x/\nu$ ranges from 0 to 1.2×10^4 across the picture and Q ranges from 0 to -9Ω with Ω in rad s^{-1}.

U_-/U_+ was in the range 0.6 to 0.7 for most of the photos. Later flow visualization experiments with lower U_-/U_+, as in the quantitative experiments, indicated that the main features were the same as shown in the photos. Figure 6(*c*) has the lower U_-/U_+ of 0.45.

Figure 4 shows two cases with $\Omega = 0$. Roller eddies are prominent as expected. Some differences between the two pictures can be seen; they have been chosen as fairly extreme cases to illustrate the extent of non-repeatability. Effects of rotation that are slighter than this difference may not be significant.

Figure 5 shows examples of flows with clockwise rotation (positive Q). In figures 5(*b*) and 5(*d*) sets of five pictures taken at 2 s intervals are shown. This interval is about 0.6 times the time of transit through the field of view at a speed of $\frac{1}{2}(U_+ + U_-)$. It is about $\frac{1}{12}$ of the rotation period in figure 5(*b*) and $\frac{1}{3}$ in figure 5(*d*).

We shall discuss these figures in §7. However, there are some points to be noted that are not fully conveyed by the still photographs.

The growth of the roller eddies for $\Omega = 0$ (figure 4) was observed to involve the process of vortex pairing (Winant & Browand 1974), as was to be expected. Some of the observed changes with increasing rotation rate involve changes in this (though, as will be discussed in §7.4, the causal connection is open to alternative interpretations). The slower growth of the eddies for $\Omega = -0.19$ rad s^{-1} (figure 5*a*) than for $\Omega = 0$ was the result of partial suppression of pairing. At higher rotation rates, pairing became intermittent, resulting in changes in the patterns like those shown in figures 5(*b*) and 5(*d*). Such behaviour was observed consistently in the range -0.26 to -1.05 rad s^{-1}. The other feature evident in figure 5(*b*), intermittent kinking of the shear layer, occurred less consistently. Other sequences of photographs (Bidokhti & Tritton 1990) show intermittent changes in the pattern of vortices but without kinking at $\Omega = -0.26$ rad s^{-1} and intermittent changes both with and without kinking at $\Omega = -0.52$ rad s^{-1}. When kinking occurred it appeared to be linked to the vortex pairing; i.e. both kinds of change occurred simultaneously. At the highest rotation rates, the intermittent pattern changes disappeared again; i.e. figures 5(*e*) and 5(*f*) are fairly representative of the pattern observed at all times.

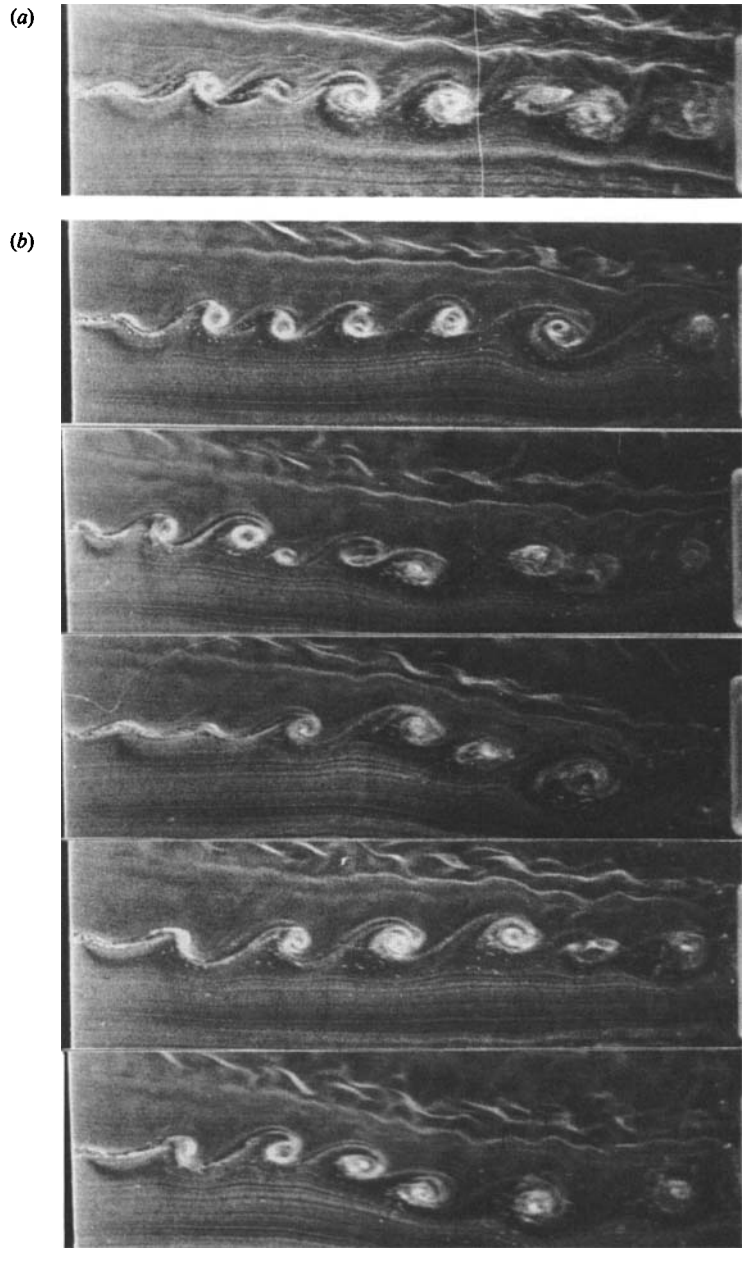

FIGURE 5(*a*, *b*). For caption see p. 481.

Figure 6 shows flows with varying rates of anticlockwise rotation (negative Q). (The fact that the shear layer is straight down the channel in figures 6(*c*) and 6(*d*) but not in figures 6(*a*) and 6(*b*) is almost certainly due to imperfections in the overall flow in the latter cases rather than being an observation of any significance.) The marked contrast with the preceding pictures will feature prominently in the interpretation in §7.

A flow with high background turbulence level could be produced by a modified arrangement of the smoothing screens (Bidokhti & Tritton 1990). Figure 7 shows

(c)

(d)

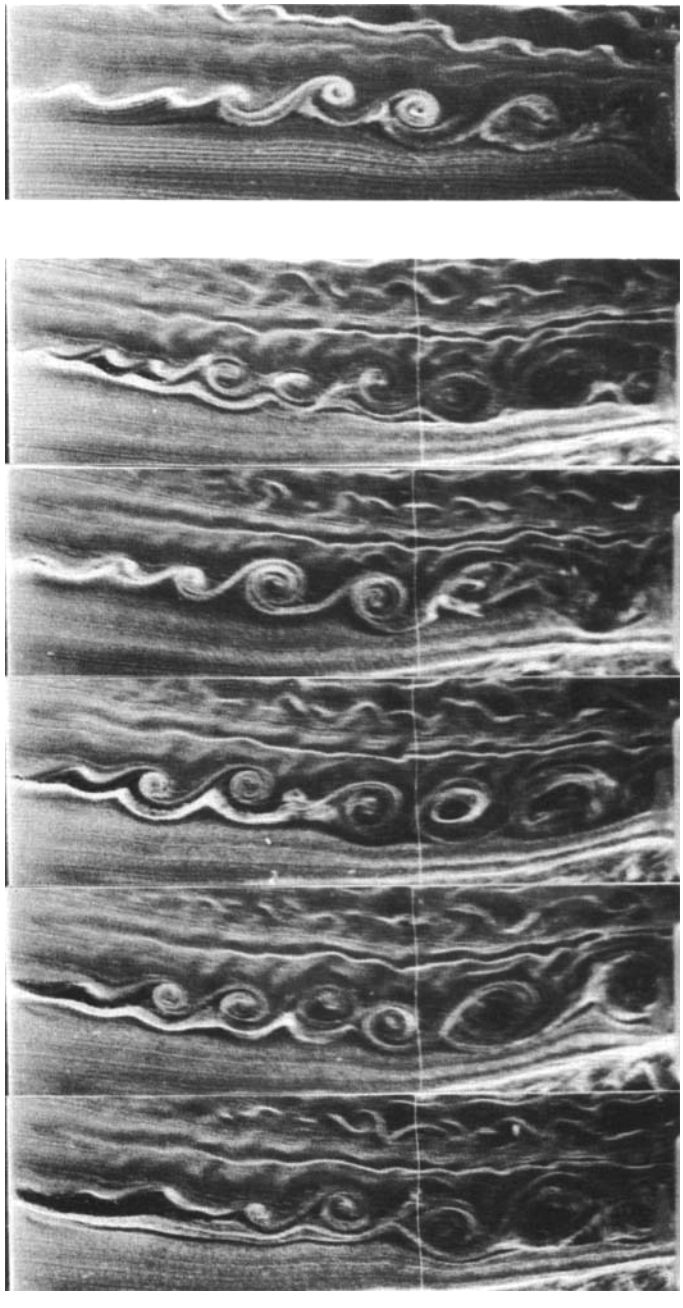

FIGURE 5(c, d). For caption see facing page.

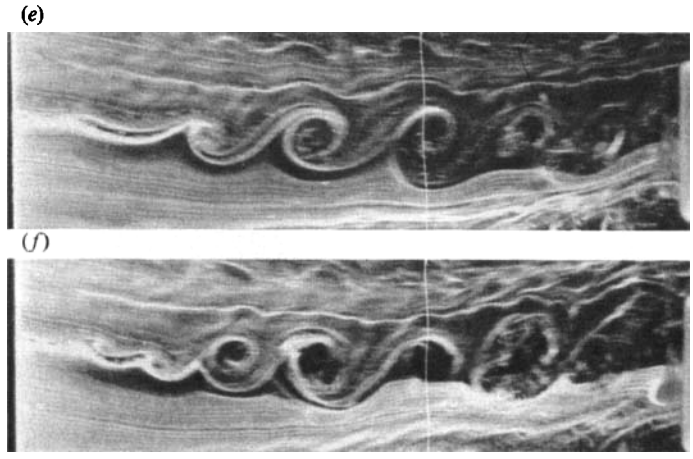

FIGURE 5. Examples of the shear layer with clockwise rotation. (*a*) $\Omega = -0.19$ rad s^{-1}, (*b*) -0.26 rad s^{-1}, (*c*) -0.52 rad s^{-1}, (*d*) -1.05 rad s^{-1}, (*e*) -1.26 rad s^{-1}, (*f*) -1.6 rad s^{-1}. Sequences of photos in (*b*) and (*d*) are at 2 s intervals.

pictures of this flow with zero and clockwise rotation. It is notable that the background turbulence has disrupted the roller-eddy structure beyond recognition in the non-rotating case, but that it is still perceptible in the rotating case.

6. Quantitative results

6.1. *The basic data*

Figure 8 shows an example of our main type of measurement: mean velocity profiles and distributions of turbulence intensity components and the Reynolds stress across the shear layer at a fixed distance downstream. Further examples are given in Bidokhti & Tritton (1990). U denotes the mean velocity and (u, v, w) the velocity fluctuation components in the usual way. Apart from correlation and spectra measurements, our main body of data consists of a large number of profiles like those in figure 8. In some cases the orientation of the hot-film anemometer was such that $\overline{u^2}$ and $\overline{w^2}$ were measured instead of $\overline{u^2}$, $\overline{v^2}$, and $\overline{uv}$. ($\overline{uw}$ should be zero by symmetry and a check that this was so within the experimental accuracy was made throughout the measurements.)

Most of the graphs below show the effect of rotation by having Q (defined and explained in §3) as abscissa. Of the dimensional quantities involved in Q, $(U_+ - U_-)$ was nominally held constant (but see below). Observations were made at both various x and various Ω. However, a large majority were made at $x = 0.425$ m with widely ranging Ω, and these provide the mainstay of our interpretation (§7). Thus Q is being used primarily as a non-dimensional form of the rotation rate, with only limited evidence presented on the consequences of other ways of varying Q. Some of the graphs include some results at $x = 0.16$ and 0.30 m. These are plotted with the origin of x, used in calculating Q, taken as the end of the splitter plate, although this is not necessarily the most appropriate choice in comparing results for different x. The Reynolds numbers corresponding to $x = 0.16$, 0.30, and 0.425 m are 1.0×10^4, 1.9×10^4, and 2.7×10^4.

The trends with Q are presented in two ways: in terms of relative quantities (for example $\overline{v^2}_{\mathrm{m}}/\overline{u^2}_{\mathrm{m}}$, where the suffix m denotes maximum value with respect to y)

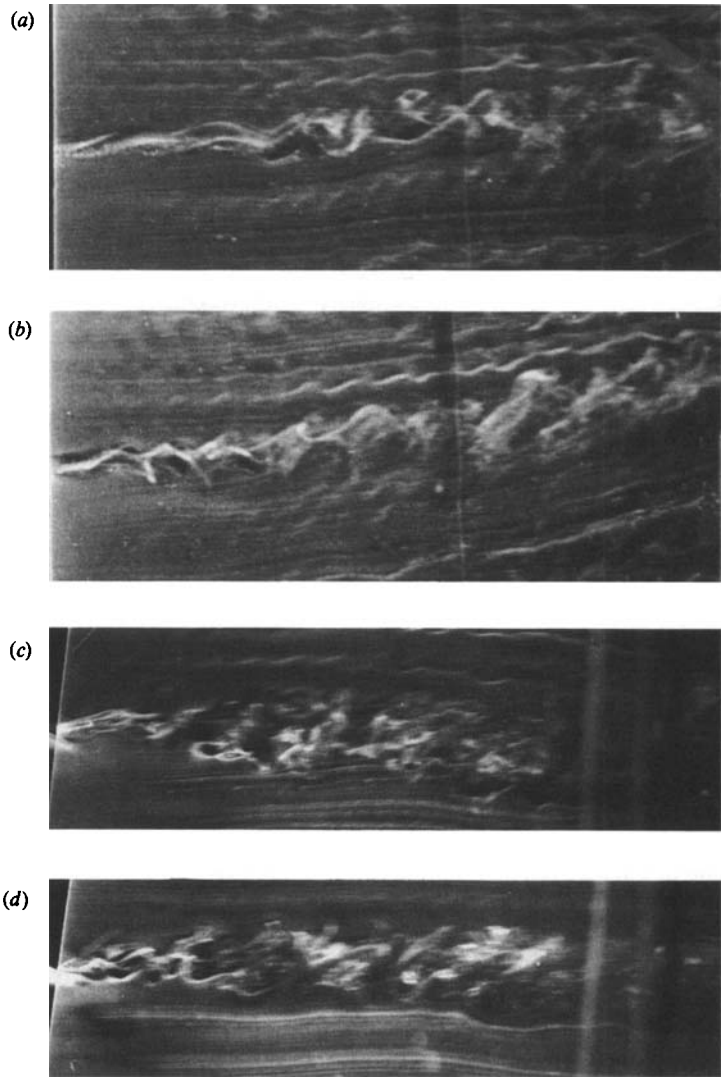

FIGURE 6. Examples of shear layer with anticlockwise rotation. (a) $\Omega = 0.16$ rad s^{-1}, (b) 0.26 rad s^{-1}, (c) 0.31 rad s^{-1}, (d) 1.05 rad s^{-1}.

in §6.3; and in terms of non-dimensionalized absolute quantities (for example $\overline{u_m^2}/(U_+ - U_-)^2$ in §6.4. The former are determined with greater accuracy than the latter, and much of the interpretation in §7 is based on these. It is fortunate that the relative quantities are just the ones that are needed for relating the results to ideas in Tritton (1992).

The reason for the poorer accuracy of the absolute quantities (additional to the fact, noted in §2, that calibration was not always frequent) was uncertainty in U_+ and U_-. It has been noted in §4 both that these may vary and that it may be difficult to specify them precisely (in ways both expected and unexpected). The measured mean velocity profiles confirm that this is a problem; the values to which they asymptote on either side of the shear layer vary (by the order of 20%) and are not always well defined. Uncertainty in U_+ and U_- causes uncertainty in the plots in §6.4 in two ways. First, they are involved directly; for example, in the non-dimensionalization of the

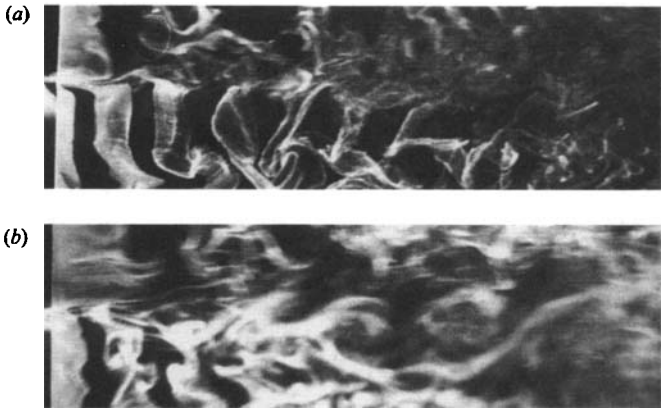

FIGURE 7. Flow visualization with high background turbulence. (*a*) $\Omega = 0$, (*b*) $\Omega = -0.40$ rad s^{-1}.

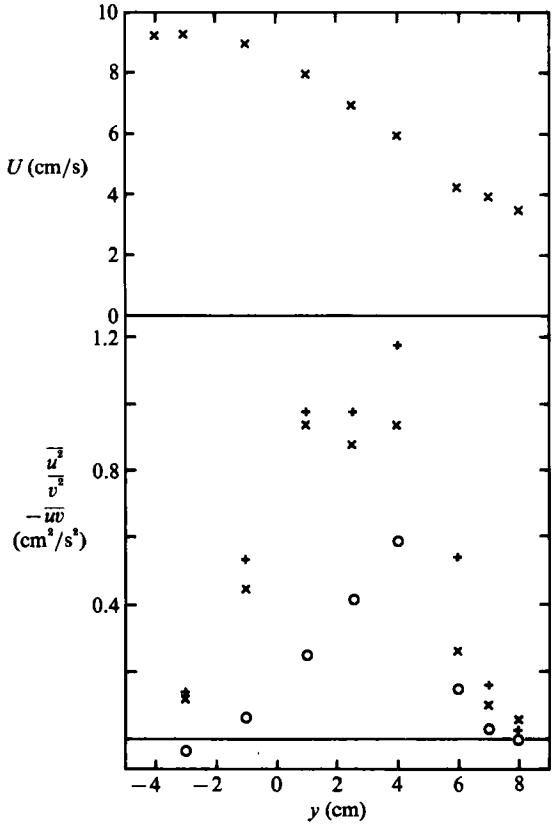

FIGURE 8. Examples of mean velocity and turbulence measurements at $x = 0.425$ m and $\Omega = 0.35$ rad s^{-1}. (Positive Ω corresponds to negative Q.) ×, U and $\overline{u^2}$; +, $\overline{v^2}$; ○, $-\overline{uv}$.

intensities or the definition of the shear-layer width. Secondly, in the non-rotating flow some of the shear-layer parameters are sensitive to U_-/U_+ (and this will presumably also be true of the rotating flow) (Rodi 1975; Brown & Roshko 1974; Saiy & Peerless 1978; Oster & Wygnanski 1982; Badri Narayanan & Raghu 1982).

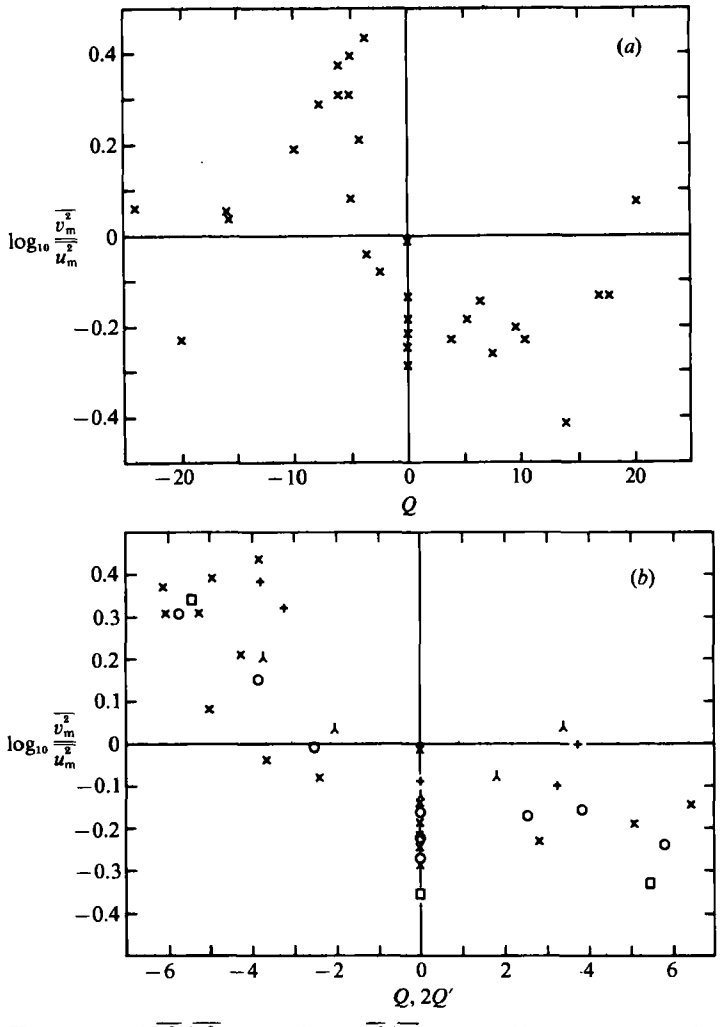

FIGURE 9. Variation of $\overline{v_m^2}/\overline{u_m^2}$ with Q (or $\overline{v^2}/\overline{u^2}$ with $2Q'$ in the case of the wake). (*a*) All measurements at $x = 0.425$ m. (*b*) ⅄, $x = 0.16$ m, +, $x = 0.30$ m, ×, $x = 0.425$ m. Open symbols are for the wake: ○, $2\Omega d/U_0 = 0.016$ (or 0), $x/d = 80$, 120, 180; □ $2\Omega d/U_0 = 0.0080$ (or 0), $x/d = 340$.

In fact, there is no clear trend of quantities such as $\overline{u_m^2}/(U_+ - U_-)^2$ with U_-/U_+ (although there are considerable discrepancies between the results of different workers). On the other hand, δ/x, where δ is some measure of the shear-layer width, varies strongly (e.g. Townsend 1975, equation (6.10.14)). Despite these limitations, the absolute quantities show trends that are important for aspects of the interpretation.

In places in the following sub-sections it is evident that further measurements of the same type would have been useful. Unfortunately we are unlikely to be able to make these measurements in the near future.

6.2. *Comparison with a wake*

Witt & Joubert (1985) present measurements of turbulence quantities in a wake in a rotating fluid. It is of interest to compare wake and shear-layer results. Because of our emphasis on relative quantities, it is useful to consider them also for the wake.

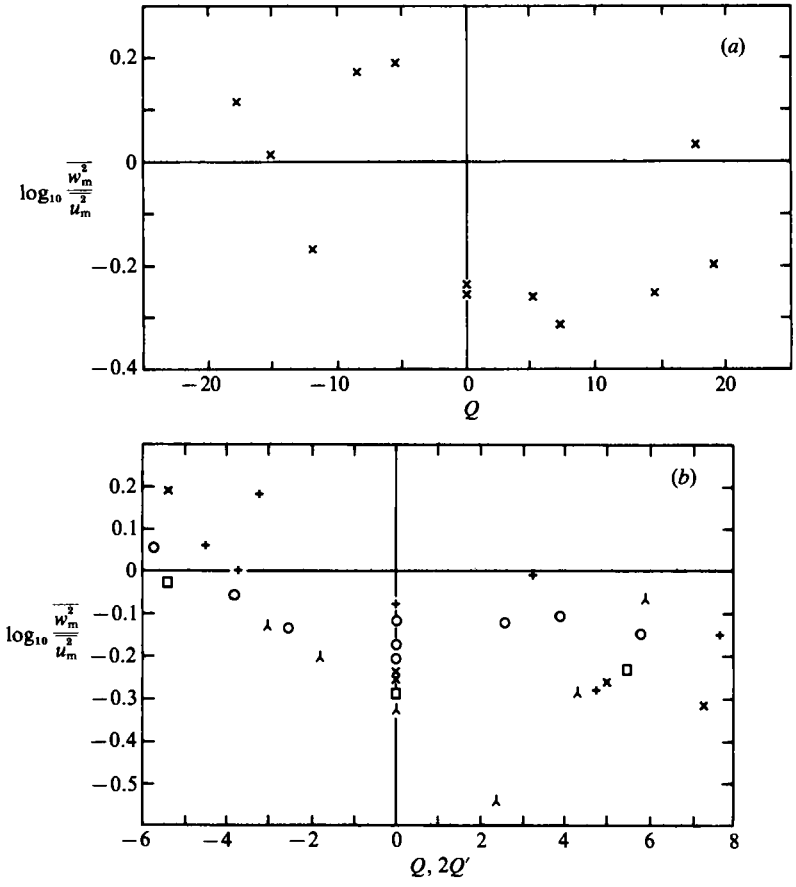

FIGURE 10. Variation of $\overline{w_m^2}/\overline{u_m^2}$ with Q (or $\overline{w^2}/\overline{u^2}$ with $2Q'$ in the case of the wake). Symbols as in figure 9.

We have calculated them from Witt & Joubert's data and include the resulting points in figures 9(*b*), 10(*b*), and 11(*b*).

The procedures for handling the wake data and thus the precise definitions of the quantities plotted are explained in Appendix A. Because of the differences between shear layers and wakes the quantities being compared are not exactly equivalent; one is looking mainly for similar trends in the two cases. A particular problem that arises in showing both cases on a single graph is how to match the scale of Q with its counterpart, $Q' = 2\Omega x/U_0$, for the wake. The reason for the matching adopted – expanding the Q'-scale by a factor of 2 relative to the Q-scale – is also explained in Appendix A but it should be noted here that this is somewhat arbitrary; there is no 'correct' choice.

6.3. *Relative quantities*

Figures 9 and 10 show ratios of maximum values of respectively $\overline{v^2}$ to $\overline{u^2}$ and $\overline{w^2}$ to $\overline{u^2}$. (Logarithmic ordinates are used so that there is symmetry between e.g. $\overline{v^2} > \overline{u^2}$ and $\overline{u^2} > \overline{v^2}$.) The maxima are inferred from profiles such as those in figure 8, with interpolation between points where appropriate. The two maxima usually occurred at approximately the same value of y (with the maximum in $\partial U/\partial y$ also close). Occasionally they were noticeably separated; the quantity plotted is always the ratio of the two maximum values, whether they were coincident or not. In each figure part

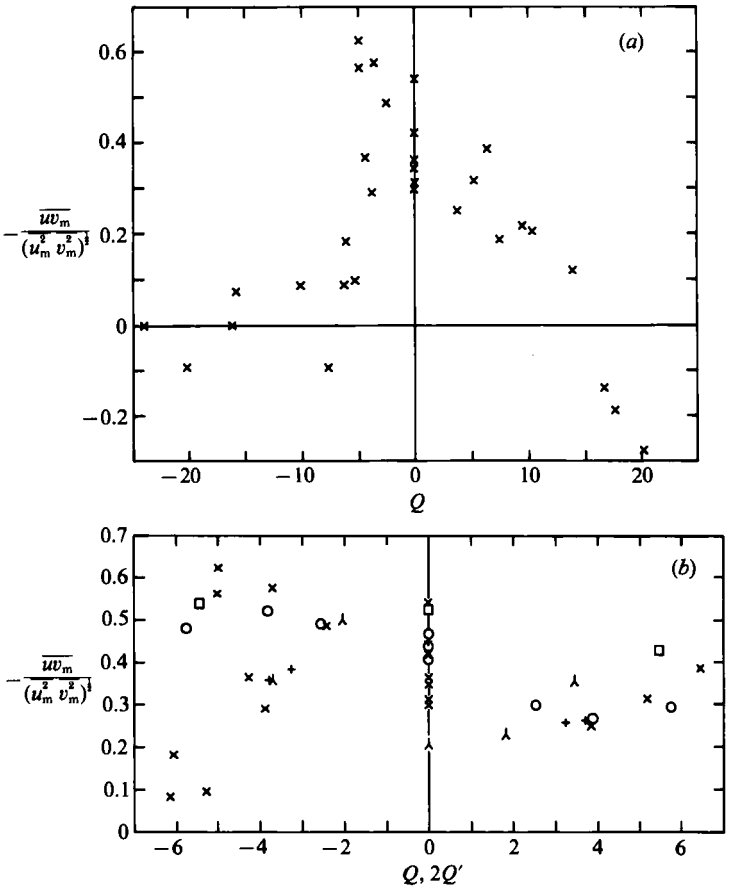

FIGURE 11. Variation of the normalized Reynolds stress with Q (or $2Q'$ in the case of the wake). Symbols as in figure 9.

(a) shows results covering a wide range of Q, all from $x = 0.425$ m. Part (b) expands the Q-scale and adds points from two other values of x; wake data (§6.2) are also added here. The larger number of points on the $\overline{v_m^2}/\overline{u_m^2}$ plots is a by-product of detailed exploration of the Reynolds stress.

In these and subsequent figures we allow the scatter of the data to indicate the size of experimental uncertainties.

So as not to focus excessively on maximum values, we also plotted graphs with the ordinate being an approximation to $\int\overline{v^2}\,dy/\int\overline{u^2}\,dy$ or $\int\overline{w^2}\,dy/\int\overline{u^2}\,dy$ (Bidokhti & Tritton 1990). The trends shown were generally similar to those in figures 9(a) and 10(a). There was one significant difference: $\int\overline{v^2}\,dy/\int\overline{u^2}\,dy$ was also greater than 1 in the range $-4 > Q > -15$ but not as large as $\overline{v_m^2}/\overline{u_m^2}$.

Figure 11(a, b) shows the normalized Reynolds stress plotted in the same way. Again the procedure has been to determine from curves such as those in figure 8 the maximum values of $-\overline{uv}$, $\overline{u^2}$, and $\overline{v^2}$, regardless of whether these all occurred at the same value of y, and then to calculate the ordinate. Again non-coincidence was generally slight and not systematic, but the procedure does mean that the quantity plotted is not necessarily exactly the normalized Reynolds stress at a particular point. It is in principle less than the normalized Reynolds stress at the position of maximum Reynolds stress and more than it at the position of maximum $(\overline{u^2}\,\overline{v^2})^{\frac{1}{2}}$.

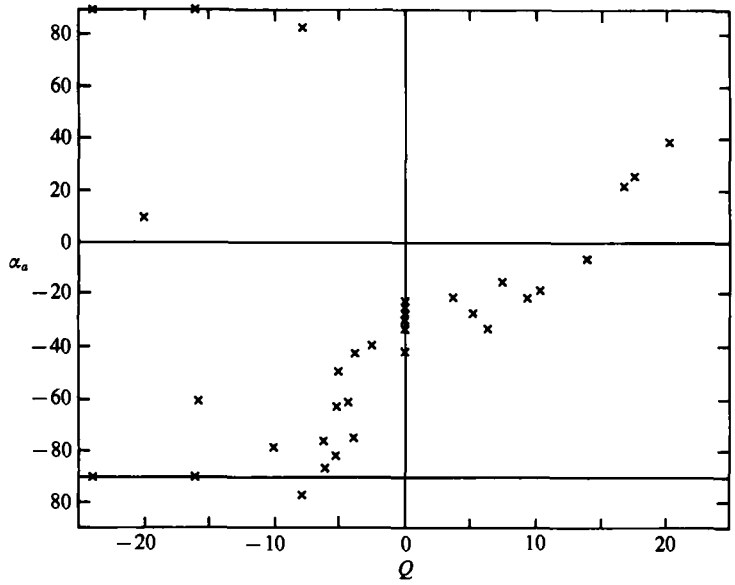

FIGURE 12. Orientation of principal axis of Reynolds stress tensor inferred from data in figures 9(*a*) and 11(*a*).

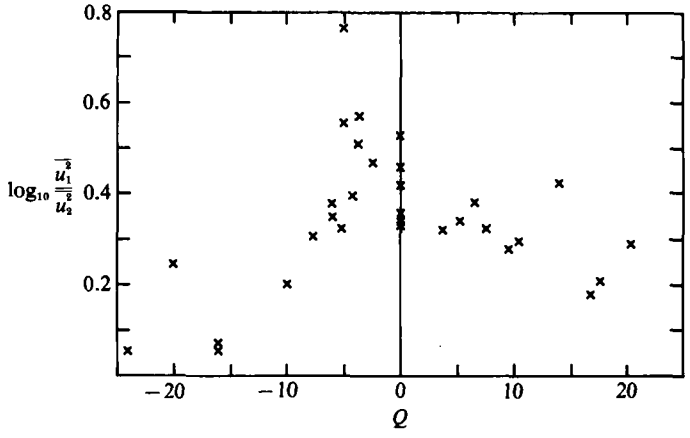

FIGURE 13. Ratio of principal components of Reynolds stress tensor inferred from data in figures 9(*a*) and 11(*a*).

A striking feature of figure 11(*a*) is the rapid drop in the normalized Reynolds stress as $-Q$ increases above about 5. We refer to this behaviour as 'Reynolds stress collapse'. We investigated this region of Q carefully to check that the collapse was a definite phenomenon. In addition to the data shown in the graphs, we carried out an experiment with a single hot-film probe inclined at 45° to the flow direction and rotated to measure sequentially $\overline{(u+v)^2}$ and $\overline{(u-v)^2}$; the difference between these before the collapse and similarity after it was very evident.

Figures 12 and 13 are derived, point by point, from the data shown in figures 9 and 11. Figure 12 shows the angle between the major principal axis of the Reynolds stress tensor and the mean flow direction; we denote this angle by α_a for consistency with the notation of Tritton (1992) and it is calculated from equation (34) of that paper.

	$\frac{U_+}{U_-}$	$\log\frac{\overline{v_m^2}}{\overline{u_m^2}}$	$\log\frac{\overline{w_m^2}}{\overline{u_m^2}}$	$-\frac{\overline{uv}_m}{(\overline{u_m^2}\,\overline{v_m^2})^{\frac{1}{2}}}$	$\log\frac{\overline{u_1^2}}{\overline{u_2^2}}$	α_a (deg.)	α_b (deg.)	α_b' (deg.)
Saiy & Peerless (1978)	0.43	−0.44	−0.27	0.52	0.68	−22	−24.5	−24.5
	0.66	−0.35	−0.08	0.51	0.61	−25.5	−26.5	−26.5
Pui & Gartshore (1979)	0.65	−0.08	—	0.53	0.52	−40	−30	−28.5
	0.75	−0.11	+0.02	0.46	0.45	−38	−31.5	−31
	0.81	+0.06	—	0.44	0.41	−50	−34	−32
Oster & Wygnanski (1982)	0.60	−0.18	−0.21	0.47	0.44	−32	−31	−31
Badri Narayanan & Raghu (1982)	0.37	−0.12	—	0.45	0.43	−36.5	−31.5	−31
	0.65*	+0.13	—	0.32	0.32	−58	−37.5	−35
Mehta *et al.* (1987)	0.50	−0.32	—	0.52	0.60	−27	−26.5	−26.5
Mehta *et al.* (1987) numerical experiment	0.50	+0.54	—	0.27	0.60	−79	−41	−26.5

* Flow still developing with x.

TABLE 1. Values of quantities plotted in the present work for shear layers in non-rotating fluids. (For the significance of α_b and α_b' see Tritton 1992.)

(Three points in figure 12 are plotted twice, two because they fall on $\alpha_a = \pm 90°$ and one because its relationship to the other points is clearer if one relaxes the convention that $-90° \leqslant \alpha_a \leqslant 90°$.) Figure 13 shows the corresponding ratio of the major and minor principal axes in the (x, y)-plane, given by equation (35) of Tritton (1992). (A log scale is used to provide direct comparability with figures 9 and 10.) When $\overline{u_1^2}/\overline{u_2^2}$ is close to 1, as it is for large $|Q|$, particularly on the negative Q side, α_a will be poorly defined; a large change in α_a may correspond to only a small change in the turbulence structure. Although figures 12 and 13 are important for a scheme in Tritton (1992), they are in no way dependent on that scheme; they are simply a reprocessing of the data to display important effects of rotation.

Figures 12 and 13 do not include the wake data. Corresponding plots for the wake appear in figures 4 and 5 of Tritton (1992).

It is natural to ask how the results for $\Omega = 0$ compare with previous work. Table 1 lists the quantities plotted in figures 9, 10, 11, 13, and 12. All data derive from laboratory experiments except the one set indicated as numerical. Wide variations reflect the fact, mentioned in §1, that there is no well-defined $\Omega = 0$ flow as a point of reference. All one can say is that our values fall satisfactorily within the range of previous measurements. (The last two columns of table 1 relate specifically to quantities involved in the scheme in Tritton (1992) and are referred to there.)

6.4. *Absolute quantities*

Figures 14 and 15 show estimates of the variations with Q of quantities that summarize profiles such as those in figure 8. Figure 14† shows the maximum values (with respect to y) of the three components of the turbulence intensity and the Reynolds stress, non-dimensionalized by $(U_+ - U_-)^2$. Figure 15 shows shear layer widths, δ_M and δ_T, based respectively on the mean velocity profile and distribution of turbulence intensity. δ_M has already been defined in §3 as the distance between the

† There are substantial differences, mainly on the negative-Q side, between figure 14 and corresponding curves in Tritton (1985). The latter were based on an early sub-set of the data, and the differences are partly due to the much fuller data we now have. However, there were some actual errors (particularly in relation to $-\overline{uv}$) in the earlier data analysis. Hence, figure 14 supersedes the earlier publication.

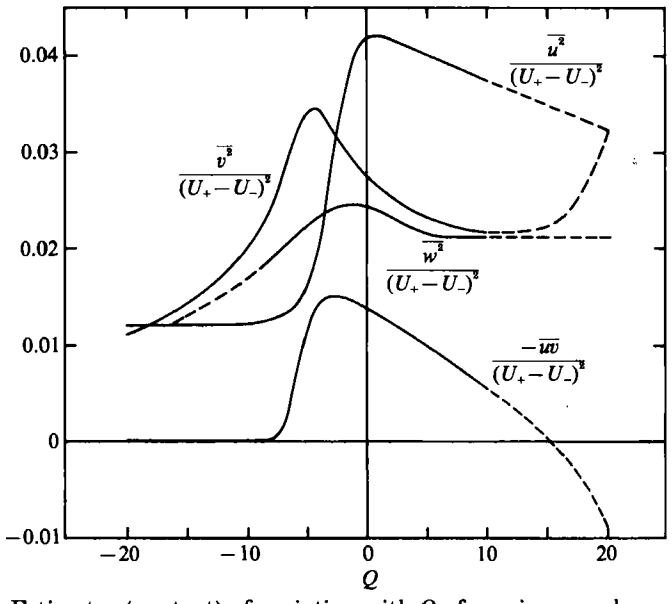

FIGURE 14. Estimates (see text) of variation with Q of maximum values of the turbulence intensity components and the Reynolds stress.

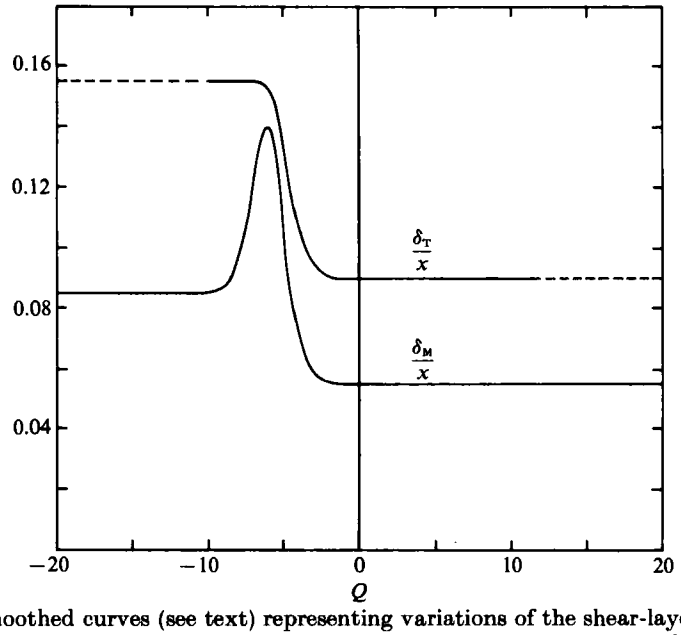

FIGURE 15. Smoothed curves (see text) representing variations of the shear-layer thickness based on the mean velocity distribution (lower curve) and turbulence intensity distribution (upper curve).

quarter and three-quarter velocity difference points. δ_T is defined as the distance between the two points at which $\overline{u^2}$ (say – see below) is half its maximum value.

Smoothed curves are shown rather than individual data points because the data are given varying weight. The curves are based in the first place on data with

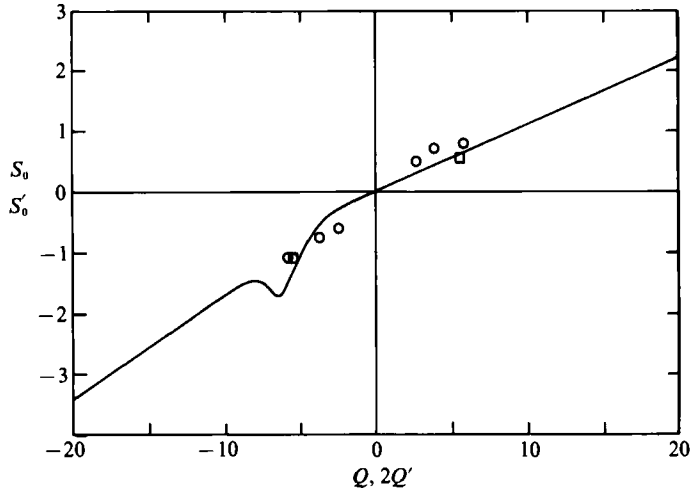

FIGURE 16. Variation of S_0 with Q for the shear layer (continuous curve) and of S_0' with Q' for the wake (points; symbols as in figure 9*b*).

frequent probe calibration checks, but data without these are also taken into account; e.g. consistency between figures 9 to 11 and figure 14 was required. The procedure is explained more fully in Bidokhti & Tritton (1990). For reasons given in §6.1, the details of the curves should be regarded with caution; parts where sparsity of data and/or poor repeatability leave the curves most in doubt are shown dashed. Within the solid parts of the curves, relative uncertainty is of the order of 20%, in the sense that trends that would still be shown if parts of the curves were shifted by 20% should be significant. (In the case of figure 15, the internal evidence implies a rather lower uncertainty, but allowance for the fact that δ/x may be expected to vary with U_-/U_+ which is itself uncertain – see §6.1 – increases the figure to around 25%.) Absolute uncertainties may be rather larger; but, in view of the wide variations in the values for $\Omega = 0$ obtained by other workers (e.g. the quantities plotted in figure 14 vary by up to a factor of 2) the significance of absolute values is in any case unclear.

In principal, three different values for δ_T are defined for the widths of each of the $\overline{u^2}, \overline{v^2}$ and $\overline{w^2}$ curves. The accuracy of the observations does not make it worthwhile showing separate trends. The procedure in drawing the curve in figure 15 was actually to consider the average of the $\overline{u^2}$ and $\overline{v^2}$ widths. For the most part no systematic difference between these two widths was perceptible. An exception is the region around $Q = -5$ for which $\overline{v_m^2}/\overline{u_m^2}$ is large (figure 9). Here, the $\overline{v^2}$ curve does become systematically narrower than the $\overline{u^2}$ curve. This is essentially the same feature as the difference between $\overline{v_m^2}/\overline{u_m^2}$ and $\int\overline{v^2}\,dy/\int\overline{u^2}\,dy$ mentioned in §6.3.

δ_M is significant not only as a measure of the shear-layer structure, but also because S_0 depends on it (§3). Figure 16 shows the S_0 versus Q curve derived from figure 15. This figure also carries S_0' versus Q' points for the wake, derived from Witt's (1986) graphs of the mean vorticity distribution. This plot forms the basis of the matching between the Q and Q' scales used also in figures 9(*b*), 10(*b*), and 11(*b*), as explained in Appendix A.

6.5. *Correlations and spectra*

The hot-film measurements included a few of correlations and spectra, all at $x = 0.42$ m.

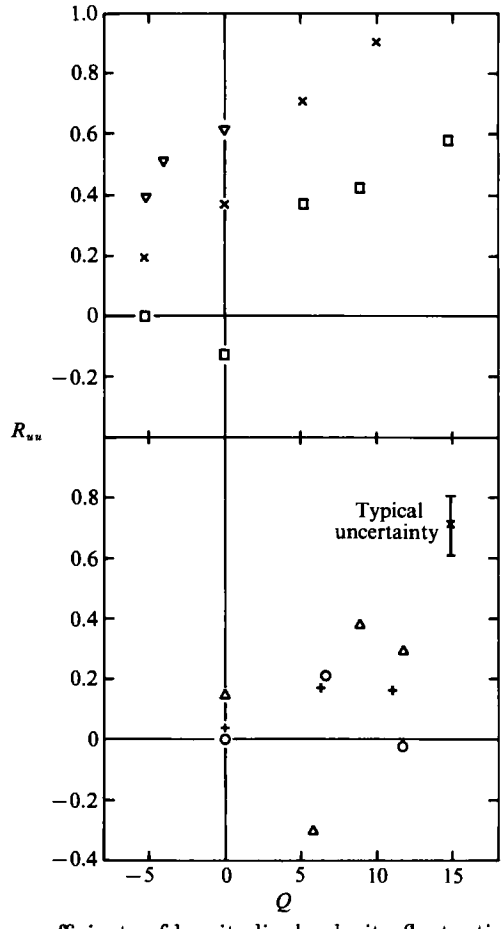

FIGURE 17. Correlation coefficients of longitudinal velocity fluctuations at two points separated in the z-direction. ▽, $r_z/x = 0.012$; ×, 0.029; □, 0.076; △, 0.107; ○, 0.18; +, 0.29.

The correlation measurements were all of the x-components of velocity at points separated in the z-direction by a distance r_z; each probe was at the centre of the shear layer in the y-direction. As explained in §2, the number was limited and not really adequate for plotting correlation curves at various rotation rates. One can, on the other hand, see the effect of rotation on the value of the correlation coefficient for various values of the probe separation. The data are shown in this way in figure 17 (this is split into two parts, each with the results for three separations, just for clarity).

Spectra of the longitudinal velocity fluctuations at the position across the shear layer where these have maximum intensity were measured for seven different rotation rates. They are shown in full in Bidokhti & Tritton (1990). Figure 18 summarizes the changes to the spectrum brought about by rotation by showing the ratio

$$\beta = \Phi_2/\Phi_1,$$

where Φ_1 and Φ_2 are the total energies in 'low' and 'high' frequency ranges. With the frequency f being non-dimensionalized as

$$F = 2xf/(U_+ + U_-)$$

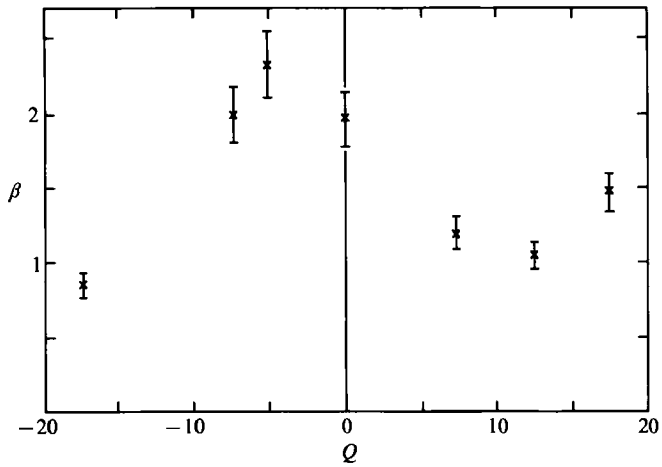

FIGURE 18. Spectral ratio as defined in text.

on the basis that the turbulence is advected past the point of observation at a speed $\frac{1}{2}(U_+ + U_-)$, and ϕ being the power spectrum normalized to

$$\int_{F_{\min}}^{F_{\max}} \phi \, \mathrm{d}F = 1,$$

Φ_1 and Φ_2 are defined as

$$\Phi_1 = \int_{F_{\min}}^{F_d} \phi \, \mathrm{d}F, \quad \Phi_2 = \int_{F_d}^{F_{\max}} \phi \, \mathrm{d}F.$$

The dividing non-dimensional frequency has been chosen as $F_d = 7.2$. On the basis that δ_M/x is typically 0.07, this corresponds to a 'wavelength' of about $2\delta_M$, which seems a convenient dividing line between 'large' and 'small' eddies. ($F_{\min}$ and $F_{\max}$ are 0.066 and 96 (Bidokhti & Tritton 1990), but the results would not be significantly different if they could be 0 and ∞.)

7. Interpretation

7.1. *Background*

The context for the interpretation of the foregoing observations is provided primarily by the concepts of stabilization of $S > 0$, destabilization for $0 > S > -1$, and restabilization for $S < -1$, discussed in Tritton (1992). Increasing positive Q will thus lead to increasing stabilization, whilst increasing negative Q will give sequential destabilization and restabilization. On the supposition that the shear-layer structure is most strongly influenced by processes in its central region where the turbulence energy production is largest and thus that S_0 is an appropriate indicator, figure 16 implies that strongest destabilization is to be expected around $Q = -3.5$, and restabilization (relative to the non-rotating flow; i.e. positive B, defined in Tritton 1992, equation (4)) when Q is less than about -5.

The terms 'stabilization' etc. have been used above without definition. In relating the experimental results to the above background, one must be more specific. An entirely two-dimensional motion is unaffected by rotation. Since the roller eddy structure prominent in the non-rotating flow is, in its basic structure, two-dimensional, one would not expect it to be suppressed by 'stabilization'. What will

be suppressed are three-dimensional motions that lead to distortion of the roller eddy structure and/or energy transfer from it to smaller-scale turbulence. One may therefore anticipate that stabilizing rotation will make the roller eddy structure more, not less, robust. Conversely, destabilizing rotation will tend to promote three-dimensional fluctuations. The theoretical immediate consequence of the shear/Coriolis interaction that lies behind the destabilization is the formation of longitudinal rolls, extended in the x-direction but involving all three components of velocity fluctuation (Tritton 1992, §2). In turbulent motion the roller eddy and longitudinal roll structures may be expected to be strongly interacting.

The companion paper (Tritton 1992) contains, in addition to discussion of general principles, consideration of the 'simplified Reynolds stress equation' or SRSE scheme for turbulent shear flows in a rotating fluid. The results of the present work, along with ones for other types of shear flow, are compared with this. Consequently, discussion of the comparison in §8 of that paper complements the interpretation below. Moreover, if one can simultaneously use the data to check the scheme and to interpret data in terms of the scheme (cf. footnote in §8 of Tritton (1992)), the results of the comparison help one to identify the important factors in the evolution of the shear layer. This applies particularly to the dynamics of the Reynolds stress collapse and the reason why the consequences of stabilization and restabilization differ.

7.2. *Principal features of the observations*

In synthesizing an interpretation from the observations of hydrogen bubbles (§5) and the quantitative data (§6) one must remember that the photographs relate entirely to a region further upstream than the station at which the majority of the measurements were made. Part of the region photographed is undoubtedly transitional rather than turbulent, although, as noted in §1, this distinction is problematic, and even the measurements at $Re = 2.7 \times 10^4$ are not in a 'fully developed' region. Nevertheless, the broad implications of the flow visualization and the measurements are similar and both contribute to the following discussion.

The most obvious single feature of the flow visualization experiments is the contrast between, on the one hand, the non-rotating and positive-Q flows and, on the other, the negative-Q flows. Roller eddies are the dominant feature of the former (figures 4, 5), whereas there is little (figure 6*a*) or no (figures 6*b–d*) sign of them in the latter. Additionally, figure 7 has shown that, when the background turbulence level is high, stabilizing rotation can make the roller eddy structure apparent when it was not for $\Omega = 0$. All these observations accord with the foregoing remarks about the way stabilization and destabilization act.

This pattern of behaviour was already known from briefer observations, with $U_-/U_+ = 0$, by Rothe & Johnston (1975). They observed that, for stabilizing rotation, the eddies persisted much further downstream than for zero or destabilizing rotation, as a consequence of a reduction of three-dimensional mixing. Destabilizing rotation enhanced three-dimensional mixing. In their pictures (their figure 4.5), the contrast between the non-rotating and stabilized cases is stronger than that between non-rotating and destabilized. This suggests a quantitative difference in the effects for $U_-/U_+ = 0$ and for our values of U_-/U_+. The different observations might, however, be due to different directions of viewing the flow. Rothe & Johnston's pictures show (x, z)-planes, in contrast to our (x, y)-views. The former could make a tendency for the eddies to become more two-dimensional particularly evident.

Direct numerical simulations, at a rather low Reynolds number, with $U_- = -U_+$ and the shear layer evolving with time (Lesieur *et al.* 1991) also show a striking

difference between very regular vortices in cyclonic flow and catastrophic disruption in anticyclonic, with the additional observation of a return to regularity at high rotation rates in the latter case.

The hot-film measurements showed considerable scatter. One contribution to this is probably the variability in the upstream region – i.e. whether or not the intermittent kinking apparent in figure 5(*b*) occurs.

Despite the scatter in figures 9–11, the main trends emerge clearly. The most prominent feature of figure 9 is the change from $\overline{v^2} < \overline{u^2}$ for non-rotating and positive-Q flow to $\overline{v^2} > \overline{u^2}$ when Q is less than about -4. This change contributes to the trends shown in figures 12 and 13 and so interpretation of these (below and in Tritton 1992) is implicitly interpretation of trends in $\overline{v^2}/\overline{u^2}$. However, we shall refer to figure 9 in the discussions below of positive- and negative-Q flows. Figure 10 shows similar but smaller changes in $\overline{w^2}/\overline{u^2}$; we refer to this in the discussion below by saying that $\overline{w^2}/\overline{u^2}$ 'follows' $\overline{v^2}/\overline{u^2}$.

The data for the normalized Reynolds stress in figure 11 are central to any interpretation. As well as the basic role of the Reynolds stress in the dynamics of any shear flow, the data are interesting as showing anticipated trends modified in unanticipated ways. It is here that the contrast, mentioned above, between the consequences of stabilization and of restabilization is most striking. Increasing Q from zero produces a steady reduction in the normalized Reynolds stress leading ultimately to a change of sign ('Reynolds stress reversal' to which we return below). In contrast, restabilization (Q less than about -6) produces a very rapid drop of the Reynolds stress to close to zero but this is not followed by significant reversal ('Reynolds stress collapse'). In figure 12 Reynolds stress reversal manifests itself by α_a becoming greater than O and Reynolds stress collapse by α_a decreasing rapidly to $-\frac{1}{2}\pi$.

The trends with Q are indicated primarily by the data at $x = 0.425$ m with Q being varied by varying Ω. The points for $x = 0.16$ and 0.30 m (figures 9*b*, 10*b* and 11*b*) are generally consistent with these trends. As noted in §3, scaling with Q alone is not necessarily appropriate, because of Reynolds-number effects and because of the initial thickness of the shear layer. Much more data would be needed to see how large the former are and how much the origin of x should be shifted. One can infer however that, qualitatively at least, increasing Ω and increasing x have similar consequences. This is of particular importance for the interpretation to be proposed in §7.5 of the Reynolds stress collapse, which supposes that it occurs as one follows a flow downstream as well as at fixed x when Ω is increased. We note therefore that we do have observations at the same rotation rate with developed Reynolds stress at $x = 0.30$ m and collapsed at $x = 0.425$ m (Q being respectively -3.75 and -5.25).

Many of the above trends are also shown by the numerical modelling of Nilsen & Andersson (1991), notably: the slight variation of $\overline{v^2}/\overline{u^2}$ with positive Q, but rapid change from less than unity to greater than unity with increasing negative Q; the tendency for $\overline{w^2}/\overline{u^2}$ to 'follow' $\overline{v^2}/\overline{u^2}$; and the contrast between a gradual decrease in the normalized Reynolds stress due to stabilization and an abrupt one due to restabilization. The most evident difference is that, in the modelling, the Reynolds stress does not change sign at large positive Q, but just drops gradually to zero. There are systematic quantitative differences between the laboratory and numerical experiments in the values of Q for the various developments; consideration of whether these are significant must await information for the numerical experiments on $S_0(Q)$, which, since it depends on the upstream history of the flow, is not necessarily the same as in the laboratory experiments.

The points on figures 9(*b*), 10(*b*) and 11(*b*) derived from the wake measurements of Witt & Joubert (1985) also show matching trends. The similarity between the two flows indicates that our interpretation has wider applicability. It also suggests that the evolution of each side of the wake is, in its broad features, little affected by the presence of the other side. The wake data cover a narrower range of rotational effects (i.e. narrower range of S) than the shear-layer data (figure 16). In particular, they do not show Reynolds stress collapse. However, figure 11 suggests that only a small extension of the range would be needed to reach this – assuming that the wake continues to behave similarly to the shear layer. It would be most interesting if the wake experiments could be so extended.

Figures 14 and 15 have been presented with caution, but some features are clear and important for the interpretation. Chief amongst these is the fact (figure 14) that the total intensity is probably rather higher for $Q > 0$ than for $-5 < Q < 0$, and is certainly not much lower. To infer, as might be natural, that the turbulence is more intense in destabilized flow than in stabilized would be incorrect.

The evolution of the shear layer width δ_M (figure 15) is, of course, determined by the Reynolds stress. One could not, however, infer all the observed trends from the appropriate curve in figure 12; nor would one expect to be able to do so, because the growth of the shear layer is determined by the full Reynolds stress profile and because the shear-layer width is the cumulative effect of growth from (and to some extent before) $x = 0$. This matter is considered more fully in Bidokhti & Tritton (1990). Here we just note two points. First, we shall be discussing below the apparent importance of the marked increase in δ_M/x in the destabilized range (and the associated increase in $|S_0|$ – figure 16) for subsequent developments. The increase in $-\overline{uv}_m/(U_+ - U_-)^2$ here is not so large (figure 14); the spreading is brought about primarily by a broader distribution of the Reynolds stress (as implied by the concurrent increase in δ_T/x – figure 15). Secondly, there are some problems in understanding why δ_M/x does not become smaller when Q is greater than about 10 and less than about -10. This may imply that the mean flow distribution is somewhat affected at large $|Q|$ by departures from two-dimensionality.

The correlation measurements (figure 17) provide information on the lengthscale of the turbulence parallel to the rotation axis. For small separations there is a very clear trend of the correlation coefficient with rotation sense and rate. For larger separations, interpretation is complicated by the occurrence of negative correlations. For $\Omega = 0$, this is in agreement with the correlation curve measured by Wygnanski *et al.* (1979) (but in disagreement with results of Badri Narayanan & Raghu 1982). It seems likely, on the basis of our limited data, that as Q becomes positive, the negative R_{uu} region continues to exist and moves to larger r_z/x. This makes any trend with Q difficult to discern when there are only a few points, but the lower part of figure 17 is still of interest as showing R_{uu} remaining significantly non-zero to large separations as Q becomes large. ($r_z/x = 0.29$ corresponds to $r_z/\delta_M \approx 5$; cf. figure 15). This observation has already been noted, in §4, in relation to possible effects of the finite height of the apparatus, but it will also be used in a more positive way in the next sub-section. The spectra are time spectra and therefore relate to the lengthscale in the flow direction. Figure 18 implies that this tends to be increased from a minimum in the destabilized range by either stabilization or restabilization (except that there is a reversal of this trend for the largest positive Q).

7.3. *Principal themes of interpretation*

Three topics are central to the interpretation to be developed in more detail in §§7.4 and 7.5.

The first is the reorientation of the turbulence shown most directly by figure 12. The occurrence of this, though not all the details, can be understood through the ideas in Tritton (1992). These ideas imply that the anisotropy, as indicated by $\overline{u_1^2}/\overline{u_2^2}$, should be largest in the destabilized range, as is observed in figure 13.

This approach focuses attention on processes in the (x, y)-plane and gives little explicit consideration to $\overline{w^2}$. The fact, noted in the preceding sub-section, that $\overline{w^2}/\overline{u^2}$ 'follows' $\overline{v^2}/\overline{u^2}$ is consistent with this. If the $\overline{w^2}$-variation had had its own distinctive features, this would have indicated aspects of the structure of the Reynolds stress tensor not covered by the ideas. In fact, it appears to be sufficient to say that, because $\overline{w^2}$ receives its energy by transfer from the other components, its size is governed by these in a way not strongly modified by the rotation.

The second topic relates to the limitations of the above, in particular the fact that it indicates no reason for asymmetry about maximum destabilization at $Q \approx -3.5$. (That is not to say that such asymmetry is in contradiction with the ideas, just that additional ideas are needed.) Our interpretation relates this to the fact that the relative effect of rotation (e.g. the value of S_0) varies with distance downstream. In particular, the markedly different consequences of stabilization and restabilization derive from the fact that the latter occurs downstream of a destabilized region.

The third topic is the varying extent to which the turbulence is fully three-dimensional or partially two-dimensional. The remarks in §7.1 about the action of stabilization and destabilization indicate the relevance of this. More generally, the tendency for strong rotation to two-dimensionalize turbulence has been demonstrated in other contexts (Hopfinger, Griffiths & Mory 1983; Hopfinger 1989).

A trend towards two-dimensionality in the stabilized flow is implied by the increasing lengthscale in the z-direction inferred from the correlation measurements. This can be seen (figure 17), despite the complication of the occurrence of negative correlations, in the increase of R_{uu} for the smaller values of r_z and in the large values of r_z/δ_{M} at which R_{uu} remains non-zero for large Q.

Such a trend has consequences that can be related to other observations, through suppression of the normal energy cascade and a trend towards 'anti-cascading' (see e.g. Lesieur 1983). Increasing lengthscale of the turbulence, in a direction perpendicular to the rotation axis, with increasing Q has been inferred from the spectra. (We will comment in §7.4 on the reversal of this trend for the final point of figure 18.) Associated with this there will be an inhibition of dissipation, consistent with the observation that the reduction in energy production implied by decreasing Reynolds stress (figures 11 and 14) is not accompanied by a comparable decrease in intensity (figure 14). (Analogous processes in homogeneous turbulence in a rotating fluid have been observed by Jacquin *et al.* 1990.)

These remarks can all be put into reverse to relate to the observations in the destabilized range. Decreased lengthscale parallel to the rotation axis is indicated by the correlations (figure 17), and is accompanied by decreased lengthscale in the flow direction indicated by the spectra (maximum β in figure 18) and by intensification of dissipation implied by the non-enhancement of intensities.

One might guess that there will be a trend back towards two-dimensionality in the restabilized range. Since no correlation measurements were made here, there is no direct evidence on this. Figure 18 provides indirect evidence: it is plausible that the

decreases in β as Q is either increased or decreased from about -5 have basically the same cause. We will consider in §7.5 whether there is evidence for inhibition of dissipation.

Two comments on the foregoing are needed. Firstly, 'two-dimensionality' refers only to the lengthscale in the z-direction becoming large, not to suppression of the z-component of the velocity fluctuation. The trend to the former is not accompanied by the latter (figure 10). A similar distinction was made by Ibbetson & Tritton (1975) and by Jacquin *et al.* (1990) for homogeneous turbulence in a rotating fluid.

Secondly, the expression 'a trend towards two-dimensionality' does not mean that the turbulence becomes effectively two-dimensional. If that happened any further increase in the rotation rate would produce no further changes in the turbulence structure (cf. Tritton 1992, §4). The observed changes, most notably those in the normalized Reynolds stress, imply that there are features of the motion that can be understood only in terms of three-dimensional processes throughout the range of Q investigated. In other words, interpretation in terms of concurrent processes of reorientation and partial two-dimensionalization of the turbulence is internally consistent only with the adjective 'partial'.

7.4. *Stabilizing rotation*

This interplay of two-dimensional and three-dimensional processes underlies the interpretation of the positive-Q behaviour in both the region of the flow visualization and the region of the measurements. Additionally, there is the fact that, even in the absence of rotation, the dominant large-scale motion is approximately two-dimensional; this perhaps makes it surprising that three-dimensional processes are as significant, in the stabilized flow, as the experimental evidence indicates.

Although the roller eddies are prominent throughout the positive-Q flow visualization experiments, there are changes in the details of the pattern as Q is increased, as shown by figure 5 and the comments on it in §5. These changes are not certainly a direct consequence of the rotation acting on the shear layer. As is shown by the data quoted near the beginning of §4, the boundary layers on the splitter plate are affected by rotation. The initial conditions from which the shear layer is formed may thus be changed; and, as discussed in §1, the flow is sensitive to these. If, on the other hand, the changes do derive directly from effects within the shear layer, then the question arises as to why the development (e.g. the rate of pairing) of approximately two-dimensional roller eddies should be affected by rotation. Probably, the smaller-scale three-dimensional motions suppressed by the rotation affect the evolution of the roller eddies. For example, on the basis of observations in Lasheras *et al.* (1986), small longitudinal vortices will have been present within the field of view of figure 4 for $\Omega = 0$; these would be strongly affected by rotation. If this is the appropriate interpretation, it suggests that theories or numerical simulations of shear layers that suppose two-dimensionality (e.g. Chollet, Lesieur & Comte 1988) should be compared with rotating, rather than non-rotating, experiments.

The interpretation of the hot-film measurements centres on the reorientation of the turbulence (figure 12), thus showing much more unambiguously that three-dimensional dynamics remain significant throughout the range of Q investigated. Since this may seem a rather surprising inference, it is worth re-emphasizing that similar trends are shown by the numerical experiments of Nilsen & Andersson (1991). The dynamics of the reorientation are discussed in Tritton (1992). However, a few points require comment here.

The observation that $\overline{v_m^2}/\overline{u_m^2}$ changes little with increasing Q (figure 9) may seem

at first sight not to fit in which the concept of reorientation. Figures 12 and 13 indicate that in fact the effect of rotation of the Reynolds stress tensor is being offset by the trend towards isotropy.

The decrease in the normalized Reynolds stress leads, at the largest Q for which we have measurements, to a change in its sign. Figures 11 (a) and 14 show that this is a natural continuation of previous trends. (It is, however, a point of difference from Nilsen & Andersson's numerical results, so it is worth noting that Reynolds stress reversal is also found in the numerical experiments on homogeneous shear flow by Bertoglio 1982 – cf. Tritton 1992, figure 2.) Discussion in Tritton (1992) (the fact that Reynolds stress reversal is not predicted by the SRSE scheme in its simplest form but is by an extended form) suggests that inhomogeneity in the flow direction (the fact that S_0 increases with distance downstream) is important for this development. The reversal implies, of course, that there is energy transfer from the turbulence to the mean flow. The likely consequences may be placed in the context of other flows that undergo relaminarization (Narasimha & Sreenivasan 1979), but could be observed only at higher Q than has been achieved and so are speculative (Bidokhti & Tritton 1990). Relaminarized flow would be unstable with respect to two-dimensional Kelvin–Helmholtz instability, so the speculations include a second generation of fluctuations (but not of turbulence).

For the most part, interpretation of the correlations and spectra is covered by §7.3. However, figure 18 shows the trend in the spectra being reversed at the highest Q for which measurements were made. The probable interpretation is that this is associated with Reynolds stress reversal; i.e. that transfer of energy from the turbulence to the mean motion is occurring preferentially in the larger eddies. However in the absence of any detectable effect of such transfer on the total intensity (figure 14), this interpretation remains speculative.

7.5. *Destabilizing and restabilizing rotation*

The main concepts in §7.3 apply also for negative Q. However, the fact that this involves sequential destabilization and restabilization makes this case more complicated.

We have already noted the almost complete disappearance of the roller eddy structure in all the negative-Q photographs. It is vestigially present at $\Omega = 0.16$ rad s^{-1} (figure 6a). Estimating S_0 in this region from earlier considerations can only be rough, because the shear-layer thickness will be influenced by the splitter-plate boundary layers; however, in the middle of figure 6(a), it is probably about -0.1. The differences between this case and the $\Omega = 0$ case (figure 4) are thus produced by, in this sense, weak rotation. For all the higher values of Ω, there is no sign of roller eddies. The turbulence appears unstructured, presumably as a consequence of the two types of instability interacting with one another, as proposed in §7.1. The sequence of pictures in figure 6 clearly shows this turbulent motion developing closer to the edge of the splitter plate as the rotation rate is increased.

The only photograph in which restabilization, in the sense that $S_0 < -1$, is reached within the field of view is figure 6 (d) for $\Omega = 1.05$ rad s^{-1}. In this, S_0 probably reaches -1 somewhere in the right-hand half of the picture, but is should be remembered that $|S|$ is larger on the edges of the shear layer. It is noticeable in this figure that the width of the turbulent region initially grows particularly rapidly but then becomes almost constant. These trends are presumably direct manifestations of destabilization and restabilization.

In channel flow (Johnston *et al.* 1972), longitudinal vortices generated by the

shear/Coriolis mechanism appear as clear structures within the turbulent motion. That we do not see this in the shear layer may just be because the orientation of our flow visualization is inappropriate. We think, however, that the concurrent presence of the Kelvin–Helmholtz mechanism results in the destabilized flow not showing such obvious coherent structures as does channel flow.

However, the fact that $\overline{u_1^2}/\overline{u_2^2}$ is largest in the destabilized range (figure 13) implies a type of 'structuring' of the turbulence. We have seen in §7.3 that this high degree of anisotropy was to be expected.

The main trends in the quantitative data for $0 > Q > -5$ have been summarized and interpreted in §7.3 as the reverse of those for $Q > 0$. There are, however, features not fully covered by this. $\overline{v_m^2}/\overline{u_m^2}$ does now show a marked change (figure 9), quickly becoming greater than 1 (a trend also shown by Witt & Joubert's wake data). This corresponds (figure 12) to rapid rotation of the principal axes, in a way relatable to the ideas in Tritton (1992). Also, as noted in different ways in §§6.3 and 6.4, this is the one range where there is a detectable difference in $\overline{v^2}/\overline{u^2}$ between the edges and the centre of the shear layer. This indicates that the structuring mentioned above is more confined to the centre of the shear layer than the ordering occurring, for example, at $\Omega = 0$. This is an understandable feature because S varies across the profile; when the destabilization is strongest at the centre, there will be significant regions on the edges of the profile where restabilization is coming in ($S < -1$). Thus, in different ways, there is evidence of decreased lengthscale in all three directions: from the correlations for the z-direction, from the spectra for the x-direction, and from the present consideration for the y-direction.

As $-Q$ is increased into the restabilizing range, the most striking feature is the Reynolds stress collapse, very different from the gradual decrease at positive Q. We interpret this difference as being a consequence of the different types of motion on which stabilization and restabilization act. In the destabilized range, there are no quasi-two-dimensional structures (or, if there are, they are not oriented approximately parallel to the rotation axis). Hence, a tendency for the rotation to impose two-dimensionality on the motion is likely to bring about a marked change in the turbulence structure rather than just a gradual one. Additionally, application of the SRSE scheme in Tritton (1992) (in particular, comparison of figures 6*a* and 6*b* there) indicates that the rapid increase of $|S|$ brought about by broadening of the shear layer in the destabilized range (figures 15 and 16 of the present paper) is a causal factor in the Reynolds stress collapse.

Beyond its collapse, with increasing $-Q$, the Reynolds stress remains close to zero, but does not show any significant sign of reversing. It is shown in Tritton (1992) that this further contrast with the behaviour for positive Q is understandable in terms of an extension to the SRSE scheme (but this understanding amounts to seeing the connections between several observed features, not to full prediction).

Collapse of the Reynolds stress implies that there is no further turbulence energy generation. The turbulence intensity decreases (figure 14). The question arises whether the rate of decrease is influenced by rotation; i.e. whether dissipation is inhibited for the same reason as it is at large positive Q. In Appendix B we estimate what the rate of decay would be if there were no such inhibition. The observed decay is slower than this, but not certainly significantly so when one allows for the approximate nature of the estimate and the uncertainties in figure 14.

8. Concluding remarks

The principal features of the observations have been listed in the Abstract. The central themes of the interpretation have been identified in §7.3. Hence, we will not repeat these here as a formal list of conclusions.

The main achievement of the experiments has been to extend study of the effect of rotation on shear flows from weak or moderately weak effect to moderately strong; i.e. to extend typical values of $|S|$ from significantly below or around unity to significantly above unity (albeit at the cost of declining data quality and some doubts about the influence of extraneous processes – such as Ekman layer effects – at the higher values). This had led to the discovery of new features, of which Reynolds stress reversal in the strongly stabilized flow and Reynolds stress collapse in the restabilized are notable. Also significant in the overall picture is the fact that stabilization and destabilization do not imply respectively less and more intense turbulence, because, one infers, dissipation is inhibited or enhanced.

Whether these features are general ones of all shear flows or are peculiar to the free shear layer is, of course, a matter for further experiments on other configurations. Our interpretations suggest that they may be of some generality. Also it is notable that, for the lower values of $|S|$ for which there are results for a wake (Witt & Joubert 1985), the two flows show remarkably similar trends.

The early stages of this experiment were carried out by Mr B. Chalk. He was unfortunately unable to continue, but his work on the design and construction of the apparatus was a most valuable contribution.

We are grateful to Professor P. Joubert of the University of Melbourne for providing additional information on the wake flow.

Appendix A. Method of presenting wake data

Data for a turbulent wake in a rotating fluid are included in several figures. These are derived from measurements by Witt & Joubert (1985) and their fuller presentation in Witt (1986). We indicate here how the wake data were handled.

The results are shown in figures 9(*b*), 10(*b*), 11(*b*) and 16 with $Q' = 2\Omega x/U_0$ as abscissa. This is the counterpart of Q. It should be noted, however, that in contrast with our results, this parameter is being varied primarily by varying x (except, of course, that the points at $Q' = 0$ correspond to $\Omega = 0$). All the rotating experiments had the same rotation rate, but measurements were made at different distances downstream, and in one case with a cylinder of different diameter; see caption to figure 9. The effect of rotation may be expected to be comparable at the same value of Q', even if $2\Omega d/U_0$ (d = cylinder diameter) is different, provided that the corresponding non-rotating wake is approximately self-preserving (Townsend 1975). Data at $x/d = 20$ were excluded because the $\Omega = 0$ results were markedly different from those further downstream owing to the proximity to the cylinder. As with the presentation of our own data, the sign of Q' is chosen to be the same as the sign of S. However, in the case of the wake, points for the same value of $|Q'|$ derive from opposite sides of the wake at the same station.

There is no specific requirement about the way the Q and Q' scales should be matched when shear-layer and wake data are plotted together. Since the most direct indication of the strength of rotational effects is the parameter S, it seemed appropriate to use scales that gave similar typical values of this at corresponding points on the abscissa. Matching was thus done on the basis of figure 16 (with S'_0 for

the wake being defined in the way analogous to S_0 for the shear layer). Since the dependences of S_0 on Q and S_0' on Q' differ somewhat, it is not possible to match precisely. But figure 16 shows that the choice of $2Q'$ matched to Q gives satisfactory average matching of S_0' with S_0 over the ranges concerned (with the constraints that the Q to Q' matching should be linear and, for convenience in reading the graphs, a rounded ratio should be chosen).

A consequence of the two-sidedness of the wake is that, although rotation makes the wake asymmetrical, the position of maximum intensity remains at or close to the centre. One does not have, for example, separate values of $\overline{v_m^2}/\overline{u_m^2}$ for the two sides. Consequently the following procedure was adopted: all quantities were taken at the positions on the two sides at which the Reynolds stress $|\overline{uv}|$ was maximum, and ratios of these calculated. For example, figure 9(*b*) shows values of $\overline{v^2}/\overline{u^2}$ at this position.

Appendix B. Decay of turbulence energy

In §7.5 the question arises whether the decay of turbulence energy after the Reynolds stress collapse is slower than it would be in the absence of rotation. At the centre of the shear layer, ignoring sideways energy transfer

$$-\frac{U_+ + U_-}{2}\frac{\partial}{\partial x}\left(\frac{\overline{q^2}}{2}\right) = \epsilon, \tag{B 1}$$

where

$$\overline{q^2} = \overline{u^2} + \overline{v^2} + \overline{w^2} \tag{B 2}$$

and ϵ is the dissipation. For a shear layer in a non-rotating fluid, the dissipation at the centre of the layer is about half the production (Townsend 1975, §6.6):

$$\epsilon_0 \approx -\tfrac{1}{2}\overline{uv}\frac{\partial U}{\partial y} = -\frac{\overline{uv}(U_+ - U_-)}{4\delta_M}. \tag{B 3}$$

We consider what decay rate would occur if

$$\epsilon \sim \epsilon_0. \tag{B 4}$$

This gives

$$\frac{\partial \overline{q^2}}{\partial x} \sim \frac{\overline{uv}_0 (U_+ - U_-)_0}{\delta_{M0}\,(U_+ + U_-)}, \tag{B 5}$$

where values with the suffix 0 apply to $\Omega = 0$ and others apply to the rotating flow under consideration. On the supposition that the trends with Q apply to the effect of varying x at fixed Ω as well as to that of varying Ω,

$$\frac{\partial \overline{q^2}}{\partial x} = \frac{|Q|}{x}\frac{\mathrm{d}\overline{q^2}}{\mathrm{d}|Q|}. \tag{B 6}$$

Hence, (B 5) becomes

$$\frac{1}{\overline{q^2}}\frac{\mathrm{d}\overline{q^2}}{\mathrm{d}|Q|} \sim \frac{\overline{uv}_0}{\overline{q^2}}\frac{x}{\delta_{M0}}\frac{(U_+ - U_-)_0}{(U_+ + U_-)}\frac{1}{|Q|}. \tag{B 7}$$

Using observed values (figures 14, 15), the right-hand side of (B 7) is about -0.2 at $Q = -10$, a factor of about 4 larger than the actual decay rate indicated by figure 14.

REFERENCES

ANDERSSON, H. I., NILSEN, P. J., ELIASSON, P. & RIZZI, A. 1988 *Proc. 14th IAHR Symp. on Progress within Large and High-Specific Energy Units*, vol. 2, p. 479. Trondheim: Tapir.

BADRI NARAYANAN, M. A. & RAGHU, S. 1982 *Dept. Aero. Engng. Indian Inst. Sci. Bangalore Rep.* 82FM4.

BERNAL, L. P. & ROSHKO, A. 1986 *J. Fluid Mech.* **170**, 499.

BERTOGLIO, J. P. 1982 *Am. Inst. Aero. Astro. J.* **20**, 1175.

BIDOKHTI, A. A. & TRITTON, D. J. 1990 *University of Newcastle upon Tyne, Dept. Phys. Rep.* GFD 90/1.

BREIDENTHAL, R. 1981 *J. Fluid Mech.* **109**, 1.

BROWAND, F. K. & LATIGO, B. O. 1979 *Phys. Fluids* **22**, 1011.

BROWN, G. L. & ROSHKO, A. 1974 *J. Fluid Mech.* **64**, 775.

CANTWELL, B. J. 1981 *Ann. Rev. Fluid Mech.* **13**, 457.

CHANDRSUDA, C., MEHTA, R. D., WEIR, A. D. & BRADSHAW, P. 1978 *J. Fluid Mech.* **85**, 693.

CHOLLET, J. P., LESIEUR, M. & COMTE, P. 1988 *Fluid Dyn. Res.* **3**, 315.

HOPFINGER, E. J. 1989 In *Theoretical and Applied Mechanics, (Proc. 17th Internat. Congr. Appl. Mech., Grenoble)* (ed. P. Germain, M. Piau & D. Caillerie), p. 117. Elsevier.

HOPFINGER, E. J., GRIFFITHS, R. W. & MORY, M. 1983 *J. Méc. Théor. Appl., Numéro Special*, p. 21.

IBBETSON, A. & TRITTON, D. J. 1975 *J. Fluid Mech.* **68**, 639.

JACQUIN, L., LEUCHTER, O., CAMBON, C. & MATHIEU, J. 1990 *J. Fluid Mech.* **220**, 1.

JIMENEZ, J. 1983 *J. Fluid Mech.* **132**, 319.

JOHNSTON, J. P., HALLEEN, R. M. & LEZIUS, D. K. 1972 *J. Fluid Mech.* **56**, 533.

KOYAMA, H., MASUDA, S., ARIGA, I. & WATANABE, I. 1979 *Trans. ASME* A: *J. Engng Power* **101**, 23.

KRISTOFFERSON, R. & ANDERSSON, H. I. 1992 *J. Fluid Mech.* (submitted)

LASHERAS, J. C., CHO, J. S. & MAXWORTHY, T. 1986 *J. Fluid Mech.* **172**, 232.

LESIEUR, M. 1983 *J. Méc. Théor. Appl. Numéro Special*, p. 5.

LESIEUR, M., YANASE, S. & MÉTAIS, O. 1991 *Phys. Fluids* A **3**, 403.

MEHTA, R. D., INOUE, O., KING, L. S. & BELL, J. H. 1987 *Phys. Fluids* **30**, 2054.

NARASIMHA, R. & SREENIVASAN, K. R. 1979 *Adv. Appl. Mech.* **19**, 221.

NILSEN, P. J. & ANDERSSON, H. I. 1991 Extended abstract: 'Plane mixing layer subject to system rotation', privately communicated.

OSTER, D. & WYGNANSKI, I. 1982 *J. Fluid Mech.* **123**, 91.

PUI, N. K. & GARTSHORE, I. S. 1979 *J. Fluid Mech.* **91**, 111.

RODI, W. 1975 In *Studies of Convection* (ed. B. Launder), vol. 1, p. 79. Academic.

ROSHKO, A. 1976 *Am. Inst. Aero. Astro. J.* **10**, 1349.

ROTHE, P. H. & JOHNSTON, J. P. 1975 *Dept. Mech. Engng, Stanford Univ. Rep.* PD-17.

ROTHE, P. H. & JOHNSTON, J. P. 1979 *Trans. ASME* I: *J. Fluids Engng* **101**, 117.

SAIY, M. & PEERLESS, S. J. 1978 *J. Fluid Mech.* **89**, 709.

SPEZIALE, C. G. & MAC GIOLLA MHUIRIS, N. 1989 *Phys. Fluids* A **1**, 294.

TOWNSEND, A. A. 1975 *The Structure of Turbulent Shear Flow* (2nd edn). Cambridge University Press.

TRITTON, D. J. 1978 In *Rotating Fluids in Geophysics* (ed. P. H. Roberts & A. M. Soward), p. 105. Academic.

TRITTON, D. J. 1985 In *Turbulence and Predictability in Geophysical Fluid Dynamics and Climate Dynamics* (ed. M. Ghil), Soc. Italiana Fis. Course XXXVIII, p. 172. North-Holland.

TRITTON, D. J. 1992 *J. Fluid Mech.* **241**, 503–523.

WATMUFF, J. H., WITT, H. T. & JOUBERT, P. 1985 *J. Fluid Mech.* **157**, 405.

WINANT, C. D. & BROWAND, F. K. 1974 *J. Fluid Mech.* **63**, 237.

WITT, H. T. 1986 Effects of rotation on turbulent boundary layers and wakes. Ph.D. thesis, University of Melbourne.

WITT, H. T. & JOUBERT, P. N. 1985 In *Preprints: 5th Symp. on Turbulent Shear Flows, Cornell*, pp. 21–25.

WYGNANSKI, I., OSTER, D., FIELDER, H. & DZIOMBA, B. 1979 *J. Fluid Mech.* **93**, 325.